VILNIUS UNIVERSITY

Dovilė
ŽILĖNAITĖ

Assessing Immunohistochemistry Biomarkers in the Spatial Context of the Microenvironment of Hormone Receptor-Positive Ductal Breast Carcinoma by Digital Image Analysis

SUMMARY OF DOCTORAL DISSERTATION

Medicine and Health Sciences,
Medicine (M 001)

VILNIUS, 2021

This dissertation was written between 2015 and 2020 at the National Center of Pathology, affiliate of Vilnius University Hospital Santaros Klinikos. The research was supported by the Research Council of Lithuania (the doctoral studies were financed from the EU structural funds).

Academic supervisor
prof. dr. Arvydas Laurinavičius (Vilnius University, Medicine and Health Sciences, Medicine, M 001).

Dissertation Defence Panel:
Chairman – **prof. dr. Jolanta Gulbinovič** (Vilnius University, Medicine and Health Sciences, Medicine, M 001).
Members:
prof. dr. Dainius Characiejus (Vilnius University, Medicine and Health Sciences, Medicine, M 001).
prof. dr. Virginija Grabauskienė (Vilnius University, Medicine and Health Sciences, Medicine, M 001).
prof. habil. dr. Dalia Pangonytė (Lithuanian University of Health Sciences, Medicine and Health Sciences, Medicine, M 001).
prof. dr. Darren Treanor (University of Leeds, United Kingdom, Medicine and Health Sciences, Medicine, M 001).

The dissertation will be defended at a public meeting of the Dissertation Defence Panel at 12 p.m. on 20th of May 2021 in the *Microsoft Teams* program in the National Center of Pathology, Affiliate of Vilnius University Hospital Santaros Klinikos, auditorium. Address: P. Baublio str. 5, Vilnius, Lithuania.

The text of this dissertation can be accessed through the library of Vilnius University as well as on the website of Vilnius University: *www.vu.lt/lt/naujienos/ivykiu-kalendorius*

VILNIAUS UNIVERSITETAS

Dovilė
ŽILĖNAITĖ

Imunohistocheminių biožymenų tyrimai hormonų receptorių teigiamos duktalinės krūties karcinomos mikroaplinkos erdviniame kontekste skaitmeninės vaizdo analizės metodu

DAKTARO DISERTACIJOS SANTRAUKA

Medicinos ir sveikatos mokslai,
Medicina (M 001)

VILNIUS, 2021

Disertacija rengta 2015–2020 metais Valstybiniame patologijos centre, VšĮ Vilniaus universiteto ligoninės Santaros klinikų filiale. Mokslinius tyrimus rėmė Lietuvos mokslo taryba (doktorantūra buvo finansuojama ES struktūrinių fondų lėšomis).

Mokslinis vadovas
prof. dr. Arvydas Laurinavičius (Vilniaus universitetas, medicinos ir sveikatos mokslai, medicina, M 001).

Gynimo taryba:
Pirmininkas – **prof. dr. Jolanta Gulbinovič** (Vilniaus universitetas, medicinos ir sveikatos mokslai, medicina, M 001).
Nariai:
prof. dr. Dainius Characiejus (Vilniaus universitetas, medicinos ir sveikatos mokslai, medicina, M 001).
prof. dr. Virginija Grabauskienė (Vilniaus universitetas, medicinos ir sveikatos mokslai, medicina, M 001).
prof. habil. dr. Dalia Pangonytė (Lietuvos sveikatos mokslų universitetas, medicinos ir sveikatos mokslai, medicina, M 001).
prof. dr. Darren Treanor (Lidso universitetas, Jungtinė Karalystė, medicinos ir sveikatos mokslai, medicina, M 001).

Disertacija ginama viešame Gynimo tarybos posėdyje 2021 m. gegužės mėn. 20 d. 12 val. *Microsoft Teams* programoje Valstybinio patologijos centro, VšĮ Vilniaus universiteto ligoninės Santaros klinikų filialo, auditorijoje. Adresas: P. Baublio g. 5, Vilnius.

Disertaciją galima peržiūrėti Vilniaus universiteto bibliotekoje ir Vilniaus universiteto interneto svetainėje adresu:
www.vu.lt/lt/naujienos/ivykiu-kalendorius

ABBREVIATIONS

AshD – Ashman's D
BC – breast cancer
CI – confidence interval
CM – the center of mass
d – density
DIA – digital image analysis
ER – estrogen receptor
G – histological grade
HER2– human epidermal growth factor receptor 2
HR – hazard ratio
HRBC – hormone receptor-positive invasive ductal breast carcinoma
IHC – immunohistochemistry
IM – invasive margin
IZ – interface zone
$IZ_{3/5/7/9}$ – 3/5/7/9-hexagon wide interface zone
LR – likelihood ratio
KMO – the Kaiser-Meyer-Olkin measure
OS – overall survival
pN – lymph node metastasis status
PR – progesterone receptor
pT – tumor invasion stage
S – stroma part
SATB1– special AT-rich sequence-binding protein 1
T – tumor part
TE – tumor edge
$TE_{1/3}$ – 1/3-hexagon wide interface zone
TIL – tumor-infiltrating lymphocytes
TME – tumor microenvironment
TNM – tumor-node-metastasis staging system

1. INTRODUCTION

1.1 Background

Breast cancer (BC) is one of the most prevalent malignant tumors and the most common cause of cancer death among women [1-5]. According to the International Agency for Research on Cancer [5, 6], in 2018, there were 2 088 849 newly diagnosed BC cases, and 626 679 women have died. Despite the advent of new technologies and a better understanding of tumorigenesis, immunohistochemistry (IHC) for estrogen receptor (ER), progesterone receptor (PR), human epidermal growth factor receptor 2 (HER2), and Ki67, and morphological features detection such as tumor size (pT), grade, lymph nodes involvement (pN), and the histologic type, are current clinical practice to predict prognosis and therapy response in BC patients [7-9]. However, due to BC heterogeneity, prognosis and treatment responses differ significantly even in patients with the same clinical symptoms and pathological characteristics. Therefore, other essential aspects and biomarkers in defining tumors and patient prognosis must be considered to improve disease management in BC patients.

Significant progress in cancer biology and translating the knowledge into personalized therapies has been made [10]. While the broad spectrum of the therapies mainly targets cancer cells, their clinical utility is hampered by heterogeneity and divergence of cancer cell populations in individual tumors [11]. Studies [12-16] highlighted the critical importance of the tumor microenvironment (TME) with complex interplay of processes involved in epithelial-mesenchymal transition of cancer cells, angiogenesis, and metastasis. Furthermore, dysregulated immune responses and interactions between cells in the TME affect tumor progression and prognosis. Therefore, comprehensive analysis of local profiles of cancer cells and TME properties may reveal the dynamics of the interactions which could be associated with prognostic and predictive data.

Essential element of the TME is tumor-infiltrating lymphocytes (TIL) which have been associated with a better prognosis in various tumors since 19th century [17, 18]; however, only recently their clinical value has been demonstrated by digital pathology tools [19-21].

A study [20] of the immune contexture in colorectal cancer with the application of digital image analysis (DIA) of IHC slides revealed the high prognostic value of CD3+ and CD8+ lymphocyte densities in central and peripheral compartments of cancer tissue. The discovery was translated into a clinically validated test (Immunoscore®), which proved to be an independent prognostic marker outperforming the conventional tumor-node-metastasis (TNM) staging system in distinct cancer types [19, 22, 23]. However, TIL assessment is not yet included in BC's clinical practice [24-26]. In 2017, the International Immuno-Oncology Biomarkers Working Group provided recommendations to standardize TIL assessment in various solid tumors [25, 26]. According to these guidelines, computational assessment of TIL should be carried out in hematoxylin and eosin-stained samples using the semi-quantitative method by determining spatial aspects – 1 mm wide invasive margin (IM) – an area that separates tumor tissue from the surrounding stroma [25-27]. However, TME evaluation by these recommendations is not very precise: there is no possibility to evaluate the composition of immune cells, while the quantitative and spatial assessment of TIL is very subjective and highly depends on the expert's judgment and experience. Therefore, studies [20, 21, 28-31] suggested using alternative methods like IHC, which could determine the phenotype of immune components, evaluate the exact position of TIL in the analyzed tissue and estimate local interactions of cancer and immune cells in TME. Moreover, double IHC can further enhance this method where both type of cell and its biological property could be identified [32, 33]. However, there are only a few studies [28, 34] that assess the spatial aspects of TIL by automatically separating tumor tissue regions and determining the tumor-stroma interface zone (IZ). Nevertheless, the contradictory results [29, 35-40] of the association between TIL and a BC patient's

prognosis, especially in the most common subtype of BC – hormone receptor-positive invasive ductal breast carcinoma (HRBC) – underscore that visual TIL enumeration, as described according to the guidelines, lacks precision. In contrast, TIL assessment by IHC and DIA methods would allow for an exact quantification of parameters such as object counts, surface area, and even features that may not be visually discriminated [41-43]. Besides, hexagonal tiling and spatial statistics methods proposed in previous work [44-46] to assess Ki67 heterogeneity could automatically visualize tumor tissue components, estimate the spatial distribution of TIL in the TME, and link identified key immune response parameters to the patient survival data.

Despite the progress in assessing the immune response, a fundamental question remains unanswered: why do the majority of tumors not reveal a significant immune response? The success of immunotherapies relies on the existing TIL and their density [47]. However, cancer cells synthesize various proteins, such as programmed death-ligand 1 (PD-L1), which in most cases suppresses tumor immunogenicity [48-50] and limits the effect of novel immune response-modulating therapies [51-55]. Therefore, the comprehensive analysis of local profiles of cancer cell and microenvironment properties, including antigen presentation, angiogenesis, proliferation, and other cancer hallmarks, could be translated into the dynamics of local interactions of cancer cells and TIL in the TME and enable more precise clinical prognostication in the HRBC patients.

1.2 The Aim of the Study

To explore associations between features of cancer progression and immune response in the spatial context of the tumor microenvironment.

1.3 The Objectives of the Study

1. Develop and optimize single and double IHC procedures for robust quantification and spatial analysis of biomarker expression.
2. Establish DIA and hexagonal grid subsampling methods to detect BC tissue microenvironment components, extract the tumor-stroma IZ, and measure the spatial distribution of immune cell variance inside and across the IZ.
3. Optimize indicators of the tumor, its microenvironment, immune response, and biomarker intratumour heterogeneity features for BC pathobiological and prognostic modeling.
4. Explore local cancer and microenvironment interaction patterns and correlate to pathology, clinical, and disease outcome data in a retrospective early-stage HRBC patient cohort.

1.4 Defended Statements

1. The developed BC tissue analytics methodology automatically extracts tumor-stroma IZ and allows to compute CD8+ cell density profiles across the IZ. These immunogradient indicators enable strong and independent prognostic stratification of patients with early-stage HRBC.
2. Integrated Ki67, PR, and CD8+SATB1+ IHC DIA data-based model allows prognostic stratification in the HRBC patient cohort, outperforming clinical and pathological parameters. This model reveals that Ki67 and PR intertumoral heterogeneity indicators are prognostically more informative than their expression rates. Also, the intratumoral density of CD8+SATB1+ cells indicates their role in the active antitumor immune response.

1.5 The Scientific Novelty of the Study and Implementation in Clinical Practice

1. *Methodology to extract tumor edge (TE) and tumor-stroma IZ*. In this work, TE and IZ were automatically determined by applying DIA and hexagonal grid subsampling of digitized BC tissue microscopy images. Tumor-stroma IZ detection, including its spatial ranking from the stroma-to-tumor aspect, enabled sampling adjustment of IZ width and quantification of immune cell density profiles to assess the TIL gradient towards the tumor aspect in early-stage HRBC samples.

2. *Prognostic value of immunogradient indicators*. For the first time, it was established that not only the density of CD8+ cells in the tumor compartment but also the center of mass (CM) for the mean of the CD8+ density (reflecting the directional variance of immune cells from stroma to tumor aspect of the IZ) are independent indicators of better prognosis in HRBC. Moreover, the aggregated IZ CD8+ cell response factor, calculated by the sum of the CD8+ density and CD8+ gradient factors scores, is an independent indicator of better overall survival (OS) and can predict the long-term (>5 years) survival of the patients with HRBC.

3. *Biological and prognostic value of CD8+SATB1+ cells*. By applying double IHC for SATB1 and CD8, and DIA, for the first time, the prognostic value of the epigenetic regulator protein SATB1 expressed in the intratumoral CD8+ cells in HRBC was demonstrated. CD8+SATB1+ T cells provided stronger prognostic information than CD8+ lymphocytes assessed by single IHC; SATB1 expression in CD8+ cells could reflect the activated state of immune cells.

4. *Non-linear relationship between the percentage of PR and its intertumoral heterogeneity and prognostic value of PR entropy*. The non-linear relationship between the level of PR expression and its Haralick's texture entropy revealed that HRBC

patients with a 20–80% expression rate of PR had better OS. Additionally, it was determined that Haralick's texture entropy of PR is prognostically more informative than the PR expression rate (percentage of PR positive cells in BC tissue).

5. *The multidimensional prognostic model based on DIA data*. For the first time, prognostic modeling, based entirely on the DIA of IHC images, was achieved in HRBC patients and reflected three biological and prognostically independent features of HRBC – PR expression, proliferation rate, and local immune response. These three indicators surpassed conventional clinical and pathological parameters of BC.

2. MATERIALS AND METHODS

2.1 Study Population and Tumor Characteristics

Surgically excised tumor samples were retrospectively collected from 101 patients with an early (stage I and II) HRBC. All patients were treated at the National Cancer Institute (Vilnius, Lithuania) and were investigated at the National Center of Pathology (Vilnius University Hospital Santaros Klinikos, Vilnius, Lithuania) from 2007 to 2009. The clinicopathological and follow-up characteristics are summarized in Table 1.

The study approval was granted by the Lithuanian Bioethics Committee (reference number: 40, 2007-04-26, updated on 2017-09-12); informed written consent was collected from all patients before the study entry.

Table 1. Patient and tumor clinicopathological parameters:

Patients (percent)	101 (100 %)
Age, years	
Mean (± standard deviation)	57.75 (±12.68)
Median	59
Range	27–87
Age, n (%)	
<59 years	53 (52.5 %)
≥59 years	48 (47.5 %)
Follow up, months	
Median	135
Range	17–143
Deceased, n (%)	
After 5 years	8 (7.9 %)
After 10 years	24 (23.8 %)
Histological grade (G), n (%)	
G1	23 (22.8 %)
G2	47 (46.5 %)
G3	31 (30.7 %)

Continued table.

Tumor invasion stage (pT), n (%)	
pT1	55 (54.5 %)
pT2	46 (45.5 %)
pT3 or pT4	0
Lymph node metastasis status (pN), n (%)	
pN0	54 (53.5 %)
pN1	35 (34.7 %)
pN2	9 (8.9 %)
pN3	3 (3.0 %)
Metastasis (M), n (%)	
M0	101 (100 %)
Treatment, n (%)	
Hormone therapy	88 (87,1 %)
Chemotherapy	61 (60,4 %)
Radiotherapy	85 (84,2 %)
Trastuzumab therapy	7 (6,9 %)

2.2 Tissue preparation, immunohistochemistry, and image acquisition

One formalin-fixed, paraffin-embedded block per patient with the maximum content of invasive tumor tissue was selected for IHC. Paraffin sections were cut at three μm thickness and mounted on positively charged slides (seven sections per case).

IHC staining was performed by a Roche Ventana BenchMark ULTRA automated slide staining system (Ventana Medical Systems, Tucson, United States). ER, PR, HER2, Ki67, CD8, and HIF1α were detected by single IHC using the ultraView Universal DAB Detection kit (Ventana Medical Systems), while for SATB1 and CD8 detection, double IHC on the single slide was performed; SATB1 was visualized using the ultraView Universal DAB Detection Kit, and for CD8 visualization the ultraView Universal Alkaline Phosphatase Red Detection Kit (Ventana Medical Systems) was used. Single and double IHC protocols were optimized for DIA by

changing antibody dilution and combining antibody detection systems. IHC was applied using ready-to-use antibodies for ER, PR, HER2 (SP1, 1E2, 4B5, respectively, Ventana (Tucson, United States), Ki67 (MIB-1, Dako (Glostrup, Denmark), dilution 1:200), HIF1α (EP118, Epitomics (San Mateo, United States), dilution 1:200), SATB1 (SP287, Abcam (Cambridge, United Kingdom), dilution 1:250) and antibodies against CD8 (C8/144B, Dako, dilution 1:1100). The sections were counterstained with Mayer's hematoxylin.

The IHC slides were digitized with a ScanScope XT Slide Scanner (Leica Aperio Technologies, Vista, CA, United States) at 20× objective magnification. DIA of the whole slide images was performed with the HALO (version 3.0311.174; Indica Labs, Corrales, United States). The HALO AI tissue classifier module was trained to segment tumor tissue, stroma, and background (consisting of necrosis, artifacts, and glass). Subsequently, the HALO Multiplex IHC algorithm (version 1.2) was used to detect and extract coordinates of ER, PR, Ki67, SATB1, CD8, and HIF1α positive cells. In contrast, the HALO HER2 algorithm (version 1.1) was used for HER2 positive cells. Examples of single and double IHC and DIA output images are presented in Figure 1.

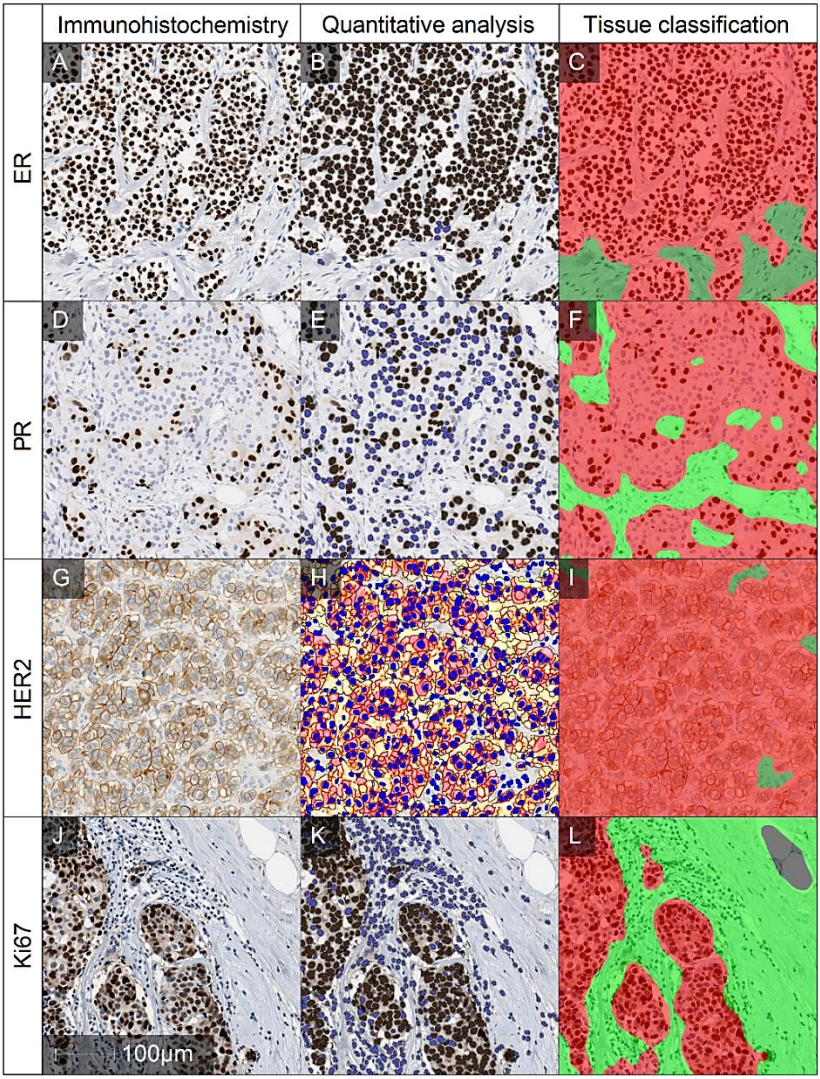

continued on next page

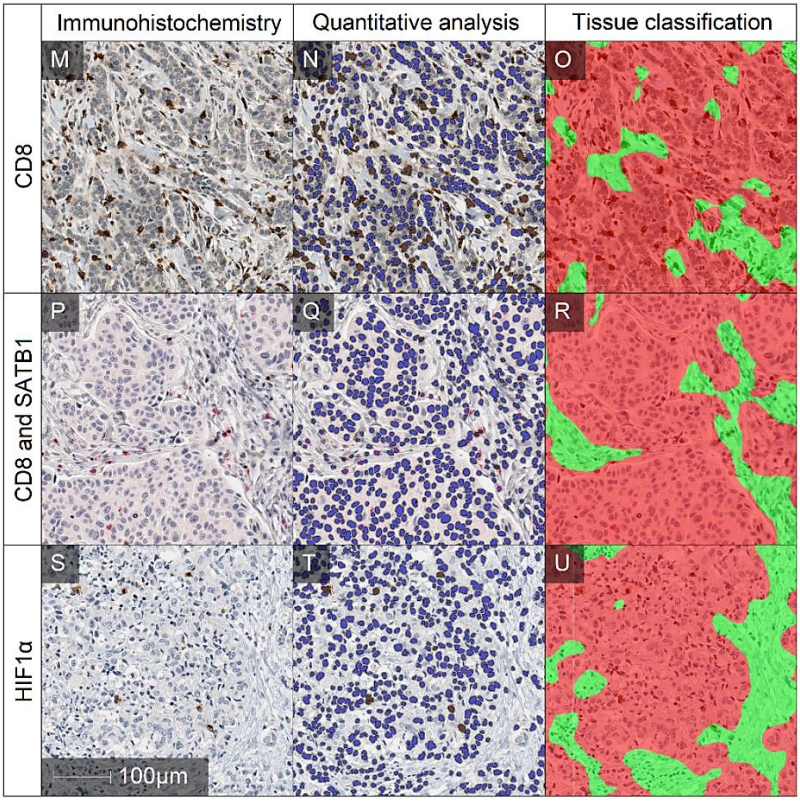

(A, B, C): IHC and corresponding DIA outputs of ER, (D, E, F) of PR, (G, H, I) of HER2, (J, K, L) of Ki67, (P, Q, R) of double IHC of CD8 and SATB1, and (S, T, U) of HIF1α. Nuclear cell segmentation algorithms mark positive (brown) and negative (blue) cells: (B) of ER, (E) of PR, (K) of Ki67. Cytoplasmic/nuclear cell segmentation algorithm marks positive HIF1α cells (T) (brown) and negative (blue) cells. HER2 cell segmentation algorithm marks negative (blue), week positive (yellow), moderate positive (orange), intense positive (red) cells of HER2 (H). Multiplex algorithm of double CD8 and SATB1 IHC (Q) separates positive CD8 (red), positive SATB1 (brown), and negative (blue) cells. (C, F, I, L, O, R, U) illustrate the automated BC tissue segmentation into the tumor (red), stroma (green), and background (black) parts by the HALO AI tissue classifier.

Figure 1. Examples of single and double immunohistochemistry and digital image analysis output images.

2.3 TE and IZ Extraction

In collaboration with our research team, a new tool was developed to automatically extract the tumor-stroma IZ and compute novel immunogradient indicators from TIL density profiles across the IZ. The method used for TE and IZ detection is explained in detail in a separate study[56]. Briefly, the IHC slides (Figure 2, A) were processed by DIA to detect tissue classes for each pixel (Figure 2, B) and extract coordinates of CD8+ positive and negative cells (Figure 2, C). According to the methodology developed by Plancoulaine et al. [45], IHC DIA data were then systematically subsampled by a randomly positioned hexagonal grid; hexagons with a side length of 65 μm were used (Figure 2, D). Coordinates of positive and negative cells, densities of CD8+ cells, and area fractions of the tumor, stroma, and background classes have been identified and calculated inside each grid element. The TE, the boundary between tumor and stroma components, was computed based on abrupt changes of tissue area fractions inside each hexagon (area fractions of the tumor, stroma, and background are presented in Figure 2, E; changes of tumor area fractions are presented in Figure 2, F and G). In Figure 2, H, the extracted TE is visualized in yellow hexagons. Grid elements not considered part of the TE were classified as either tumor, stroma, or background by the maximum of tissue area fractions. Later, the shortest distance to the extracted TE was computed for each grid element; the extracted TE hexagons had rank 0, and elements inside the tumor were ranked with their positive distance from TE, while hexagons in the stroma were assigned with their negative distance from the TE. The extracted IZ, consisting of TE with tumor and stroma tissue, were defined for different width choices; however, it was found that the IZ of width 9 (abbreviated as IZ_9, ranks [−4; 4]) with TE_3 consisting of ranks [−1; 1] (rather than TE_1 of rank 0) is optimal for HRBC. Figure 2, I shows a 9-hexagon wide IZ; tumor aspect of IZ (rank = 2, 3, and 4), stroma aspects of IZ (rank = –4, –3,

and –2), and TE (rank = –1, 0, and 1) labeled as red, green and yellow, respectively.

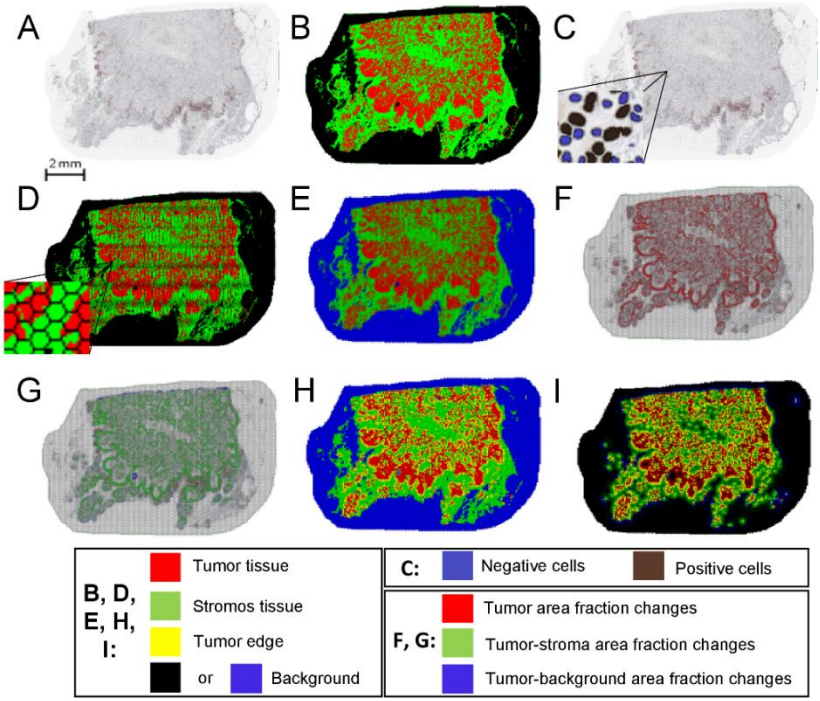

(A): input of digitized CD8+ IHC whole slide images. (B): pixel-wise classification of the BC tissue by DIA. Tumor parts are in red, stroma in green, and background in black color. (C): quantitative analysis of CD8 by DIA. The nuclear cell segmentation algorithm marks positive (brown) and negative (blue) cells of CD8. (D): hexagonal grid segmentation; hexagon side length – 65 μm. (E): area fractions of the tumor (red), stroma (green), and background (blue). (F): tumor area fraction changes (red). (G): tumor area fraction changes divided into tumor-stroma (green) and tumor-background (blue) changes. (H): detected TE (yellow). (I): IZ of 9-hexagons wide (IZ9). IZ's tumor aspect (ranks 2, 3, and 4) presented in red color, and IZ's stroma aspect (ranks –4, –3, and –2) is green, TE (ranks –1, 0, and 1) is yellow.

Figure 2. Detection steps of tumor edge and tumor-stroma interface zone in breast cancer tissue.

2.4 Computation of Immunogradient Indicators

Quantitative immune response indicators (the mean and standard deviation of CD8+ cell density in the TE, tumor, and stroma aspect of IZ) were calculated by summarizing the hexagonal CD8+ cell density values for each rank into rank quantities. The rank quantities formed a collective interface CD8+ cell density profile that reflected the distribution of immune cells in HRBC and revealed how CD8+ cell densities and their standard deviations varied inside and across the analyzed IZ. Examples of CD8+ cell density profiles for three BC tissue are shown in Figure 3.

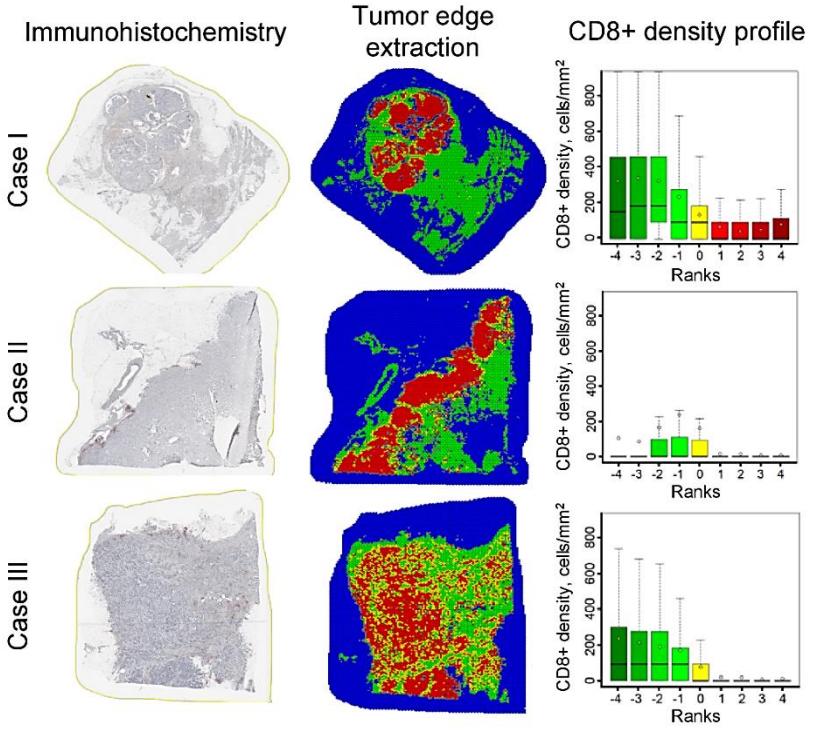

Digitized IHC slides of CD8 stained BC tissue are presented on the left. The detected TE is in yellow, the stroma is in green, the tumor is in red, and the background is in blue (center). On the right, CD8+ density profiles are

Continued figure.

presented for three different BC tissues. The box-whisker plot illustrates the mean, median, and variance of the CD8+ cell density within ranks from −4 to 4. The ranks are colored according to stroma (green), tumor (red) tissue aspects, while TE (rank 0) is presented in yellow.

Figure 3. Examples of three CD8+ cell density profiles.

Moreover, to express the directional variance of immunes cells from stroma to tumor aspect of the IZ, two indicators – the CM and immunodrop (ID) were computed. The CM was calculated using formula 1:

$$CM = \frac{\sum_{r_i} r_i \, q(r_i)}{\sum_{r_i} q(r_i)}, \quad (1)$$

where r_i represents 9 ranks in the IZ, ri $\in [-4;4]$, and $q(r_i)$ indexes the rank quantity, e.g., the mean or standard deviation of CD8+ cell density.

The CM defined the coordinate in the horizontal axis of the CD8+ cell density profile and allowed to assess the gradient of the CD8+ cells towards the tumor; if the CM value was positive, CD8+ cells were considered to infiltrate into the tumor core, and if negative, it was considered that CD8+ cells were concentrated in the stroma aspect of IZ. Meanwhile, the ID indicator represented an abrupt change of CD8+ cell density near the TE and was calculated using formula 2:

$$ID = \frac{q(r_{-1})}{q(r_1)}, \quad (2)$$

where $q(r_{-1/1})$ indexes the rank quantity in rank –1 or 1.

Accordingly, the immune response against the tumor was characterized by the following immunogradient parameters:

1) quantitative variables:

a) the mean and standard deviation of CD8+ cell density in the stroma aspect of the IZ (hexagons from rank −4 to rank –2),

b) the mean and standard deviation of CD8+ cell density in the TE (hexagons from rank −1 to rank 1),

c) the mean and standard deviation of CD8+ cell density in the tumor aspect of the IZ (hexagons from rank 2 to rank 4),

2) directional variance variables:

a) the mean and standard deviation of the CM of CD8+ cell densities,

b) the ID of CD8+ cell density.

2.5 Computation of IHC and Intratumoral Heterogeneity Indicators

To explore the prognostic value of IHC and intratumoral heterogeneity indicators in HRBC, the set of 7 IHC variables were calculated and included:

1) **global quantities of conventional BC variables per case:**
   a) the percentages of ER, PR, Ki67, and HER2 2+ and 3+ positive cells in the tumor compartment,
2) **intratumoral heterogeneity indicators:**
   a) the Haralick's texture parameters (entropy, energy, homogeneity, contrast, and dissimilarity) and Ashman's D (AshD) bimodality indicator of ER, PR, and Ki67,
3) **immune response indicators:**
   a) the densities of CD8+ and CD8+SATB1+ positive cells in tumor and stroma compartment,
4) **hypoxia-inducible properties variables:**
   a) the percentage of HIF1α positive cells in the tumor and stroma compartments.

The methodology of this part is described in detail in a separate study [57]. Variable sets 1, 3, and 4 were collected from the HALO

DIA data for each digitized IHC slide. The intratumoral heterogeneity indicators were calculated using the hexagonal tiling methodology as described above; DIA data were subsampled with 257 μm side length hexagons. Positive and negative cells of all 7 biomarkers were counted based on the DIA's cell coordinates inside each hexagon. Grid elements containing fewer than 50 cells were regarded as insufficient sampling and were not used for further analyses. Heterogeneity indicators for HER2, CD8+, CD8+SATB1+, and HIF1α were not calculated since low expression and low dynamic range was observed for all these biomarkers. Percentages of ER, PR, and Ki67 were computed for each hexagon and subsequently ranked linearly into ten intervals (level 1 (0–10%), level 2 (>10–20%), etc.) to compute the co-occurrence matrix. Heterogeneity parameters were then extracted from the co-occurrence matrix as Haralick's texture indicators (entropy, energy, homogeneity, contrast, and dissimilarity) as described in [58]. The Ashman's D (AshD) bimodality indicator was calculated for the intratumoral distributions of ER, PR, and Ki67 expression based on the search of two hidden distributions in the histogram of hexagonal grid data using Gaussian mixture models [59] and expectation-maximum algorithms [60].

2.6 Statistical Methods

A two-sided Welch's t-test was used for the homogeneity of variances comparison. Summary statistics were performed with significance tests based on one-way ANOVA with Bonferroni's post hoc test for pairwise comparisons. $\chi 2$ and Fisher's exact test were applied to estimate significant associations for non-parametric statistics. Since distributions of IHC biomarkers results revealed left asymmetry, logarithm-transformed values were used for parametric statistics; however, for readability, the prefix log is not used in the text and graphs. After data transformation, the scatter plots of the data corresponded to the normal distribution. Moreover, highly

correlated (r > 0.9) indicators were eliminated to avoid multicollinearity or singularity in multivariate survival analysis. The statistical significance was set at $p < 0.05$.

Factor analysis on a DIA data set was subsequently performed using the factoring method of principal component analysis with factors retained based on an eigenvalue >1; orthogonal varimax rotation of the initial factors was used [61]. Before factor analysis, the set of variables was evaluated using the Kaiser-Meyer-Olkin (KMO) measure – if the KMO was higher than 0.5, the variable was considered adequate, while lower KMO indicated that the variable might not be relevant for factor analysis [61-63].

A cutoff value for all continuous variables was determined by web-based Cutoff Finder software (Charité University, Berlin, Germany) [64]. The Kaplan–Meier was used to summarize OS data, and the log-rank test was applied to compare the statistical significance of OS distributions. Cox regression analysis was applied to test the independent prognostic significance of the IHC indicators in the context of clinicopathological variables. The final models' predictive value and statistical power were estimated based on the $\chi 2$ and/or likelihood ratio (LR) [65].

Due to a limited cohort size, data overfitting was minimized by leave-one-out cross-validation [66]; the most frequent variables were further tested in the Cox proportional hazard analysis.

TE and IZ extraction were performed in C++ (g++ 7.3.8) platform using libtiff (version 5.2.4; https://www.libtiff.org) and Boost (version 1.67; https://www.boost.org). Statistical analyses were completed with SAS (version 9.4; SAS Institute Inc., Cary, USA); plots were produced with R (version 3.4.4*; R Development Core Team*).

3. RESULTS

3.1 Summary Statistics of CD8+ Cell Density Indicators

After TE extraction, a detailed analysis of classified hexagons was performed to determine the maximum width of tumor-stroma IZ. It was found that that the IZ could be extended only by 4 hexagons to the tumor side; otherwise, more than 5% of analyzed cases could be lost in this HRBC cohort. Consequently, after determining the maximum width of the IZ, IZ's widths of 3, 5, 7, and 9 hexagons, abbreviated as IZ_3, IZ_5, IZ_7, and IZ_9, respectively, were tested with TE, which was consisted of hexagons with rank 0 (abbreviated as TE_1) and TE with ranks from –1 to rank 1 (abbreviated as TE_3). In this way, 7 different TE and IZ combinations were obtained and analyzed in this work. The most significant prognostic stratifications in this HRBC cohort were achieved in IZ of width 9 with TE consisting of ranks [−1; 1]. The summary statistics of CD8+ cell density indicators computed in IZ_9 with TE_3 are presented in Supplementary Table 1.

The decrease of CD8+ cell density toward the tumor aspect of IZ was observed. The distribution analysis of CD8+ cells within the IZ showed that the densities were highest and most dispersed in the stroma aspect of the IZ, less abundant and dispersed within the TE_3, and lowest and less dispersed in the tumor aspect of the IZ ($p < 0.001$) (Supplementary Table 1).

3.2 Factor Analysis of CD8+ Cell Density Indicators

Two orthogonally independent factors of CD8+ cell density indicators were extracted (Figure 4). Before this analysis, the data set was assessed using the KMO test; the overall sample adequacy measure for all variables reached 0.74. Altogether, the two factors explained 90.92% of the variance in the data set. Factor 1 was described by strong positive loadings of the variables that reflected

the level of CD8+ density within all IZ aspects and was therefore interpreted as the CD8+ density factor. Meanwhile, factor 2 was characterized by strong positive loadings of the directional variance indicators – the CM for both mean and standard deviation of the CD8+ density and strong negative loading of the ID indicator. This factor was interpreted as a CD8+ gradient factor, whereas higher factor 2 scores reflected increasing CD8+ density toward the IZ tumor aspect. Moreover, the sum of factor 1 and 2 scores was computed as aggregated IZ CD8+ cell response factor to test factors combined prognostic power.

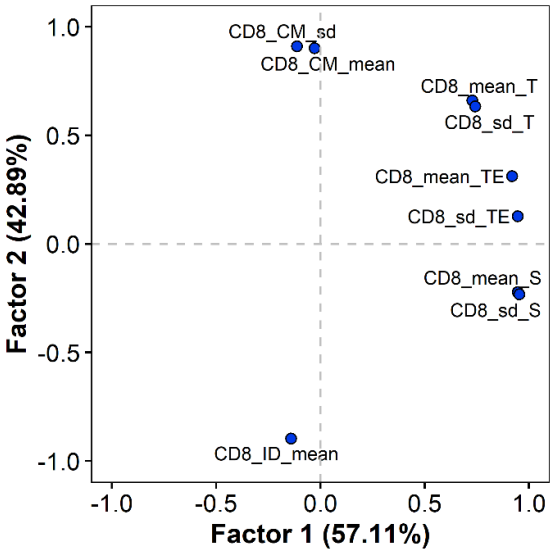

CD8_CM_mean, the center of mass for CD8 density by mean in ranks [–4; 4]; CD8_CM_sd, the center of mass for CD8 by variance in ranks [–4; 4]; CD8_ID_mean, immunodrop of the mean of CD8+ density; CD8_mean and CD8_sd (standard deviation) are summarized in the stroma aspect (S), TE, and tumor (T) aspect of IZ, respectively.

Figure 4. Rotated factor pattern of immunogradient indicators.

3.3 Prognostic Value of the Immunogradient Indicators

Univariate Kaplan-Meier analyses with a hazard ratio (HR) and log-rank test were performed to estimate the TIL density and clinicopathological indicators' prognostic potential. The patient OS probability stratifications are presented in Figure 5. Higher the CM for CD8+ density by mean, the variance of CD8+ cell density in stroma aspect, the mean and variance of CD8+ cell densities in TE and tumor aspects, CD8+ density factor, CD8+ gradient factor, and aggregated IZ CD8+ cell response factor were associated with higher OS probabilities. Worse OS was associated with the higher ID of the mean of CD8+ density. No significant stratifications were obtained for the CM for CD8+ density by variance, the mean of CD8+ cell density in stroma aspect of IZ, histological grade (HR = 1.2; 95% confidence interval (CI): 0.52–2.81; $p = 0.67$), pT stage (HR = 0.99; 95% CI: 0.45–2.22; $p = 0.99$), and pN status (HR = 2.17; 95% CI: 0.95–4.97; $p = 0.07$). Meanwhile, higher patient age was associated with worse OS (HR = 2.45; 95% CI: 1.05–5.73; $p = 0.039$).

The independent prognostic value of the immunogradient indicators was tested by multiple Cox regression analyses along with the conventional clinicopathological variables (Table 2). Two prognostic models were investigated: model 1 was produced from the age group, pathology characteristics (pT, pN, and histological grade), and the IZ CD8+ cell density indicators derived from an IZ_9 with TE_3, and model 2 was obtained by replacing the immunogradient indicators' data set with the aggregated IZ CD8+ factor score (Table 2). Model 1 showed the independent prognostic value of four indicators: better OS was predicted by the higher the CM of the CD8+ mean density and the mean of the CD8+ density in the tumor aspect of the IZ; worse OS was predicted by the higher age and pN. Model 2 revealed two independent factors – higher aggregated IZ CD8+ cell response factor score predicted better OS in the context of worse OS predicted by pN status. These two Cox regression models were validated using leave-one-out cross-

validation; the frequency of the model 1 and 2 was 98 and 63 times, respectively. The statistical significance of both models, measured by LR, was very strong: – 24.63 for model 1 ($p < 0.0001$) and 14.32 for model 2 ($p = 0.0008$).

Table 2. Statistics of multiple Cox regression analyses for correlation of the immunogradient indicators with overall survival:

Indicator	Hazard ratio	95% confidence interval	*p*-value
Model 1, LR: 24.63, $p < 0.0001$			
Age group (≤59 vs. >59)	2.54	1.06–6.13	0.0374
pN group (pN0 vs. pN1–3)	3.60	1.42–9.12	0.007
CD8_CM_mean	0.39	0.16–0.94	0.0367
CD8_mean_T	0.20	0.07–0.53	0.0014
Model 2, LR: 14.32, $p = 0.0008$			
pN group (pN0 vs. pN1–3)	2.53	1.08–5.93	0.0319
Aggregated IZ CD8+ cell response factor	0.28	0.12–0.62	0.0019

CD8_CM_mean, the center of mass for CD8 density by mean in ranks [–4; 4]; CD8_mean has summarized in tumor (T) aspect of IZ; LR, likelihood ratio.

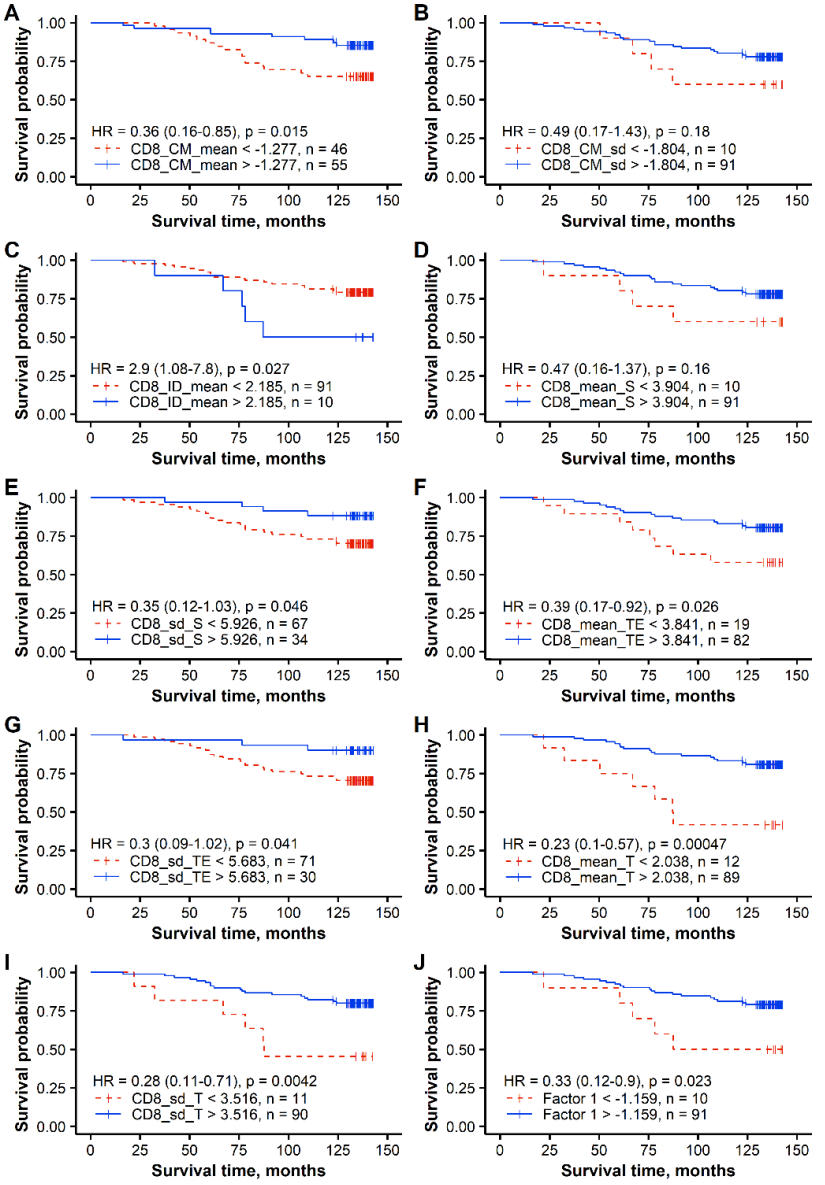

continued on next page

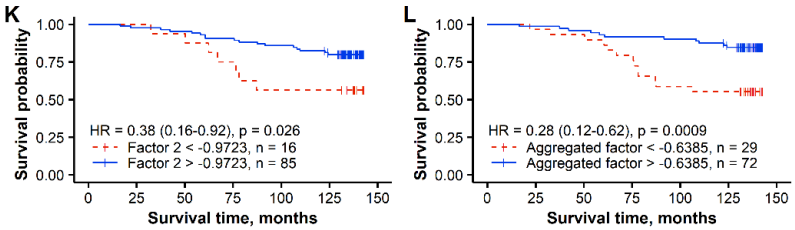

(A): the center of mass for CD8 density by mean (CD8_CM_mean) in ranks [–4; 4]; (B): the center of mass for CD8 by variance (CD8_CM_sd) in ranks [–4; 4]; (C): immunodrop of the mean of CD8+ density (CD8_ID_mean); (D): the mean of CD8+ density in the stroma aspect of IZ (S); (E): the variance of CD8+ density in the stroma aspect of IZ (S); (F): the mean of CD8+ density in the tumor edge (TE); (G): the variance of CD8+ density in the tumor edge (TE); (H): the mean of CD8+ density in the tumor aspect (T); (I): the variance of CD8+ density in the tumor aspect of IZ; (J): CD8+ density factor (factor 1); (K): CD8+ gradient factor (factor 2); (L): aggregated IZ CD8+ cell response factor (aggregated factor).

Figure 5. Kaplan-Meier survival curves with a hazard ratio (HR) and log-rank test for correlation of the immunogradient indicators with overall survival.

3.4 Summary Statistics and Prognostic Value of the IHC and Intratumoral Heterogeneity Indicators

The summary statistics of quantitative IHC biomarkers and their intratumoral heterogeneity indicators are presented in Supplementary Table 2.

Univariate Kaplan-Meier analyses with an HR and log-rank test were performed to estimate the conventional BC IHC, immune response, hypoxia-inducible, and intratumoral heterogeneity indicators' prognostic value. The patient OS probability stratifications are presented in Figure 6. The higher expression rate of PR and HER2 in the tumor tissue, immune cells densities of CD8+ and CD8+SATB1+ in the stroma and tumor parts, ER and PR entropy, and PR AshD bimodality were associated with higher OS probabilities. Worse OS was associated with a higher ER expression

and Ki67 AshD bimodality indicator. No significant stratifications were obtained for the percentage of Ki67 and HIF1α, ER AshD bimodality indicator, and Haralick's texture entropy of Ki67.

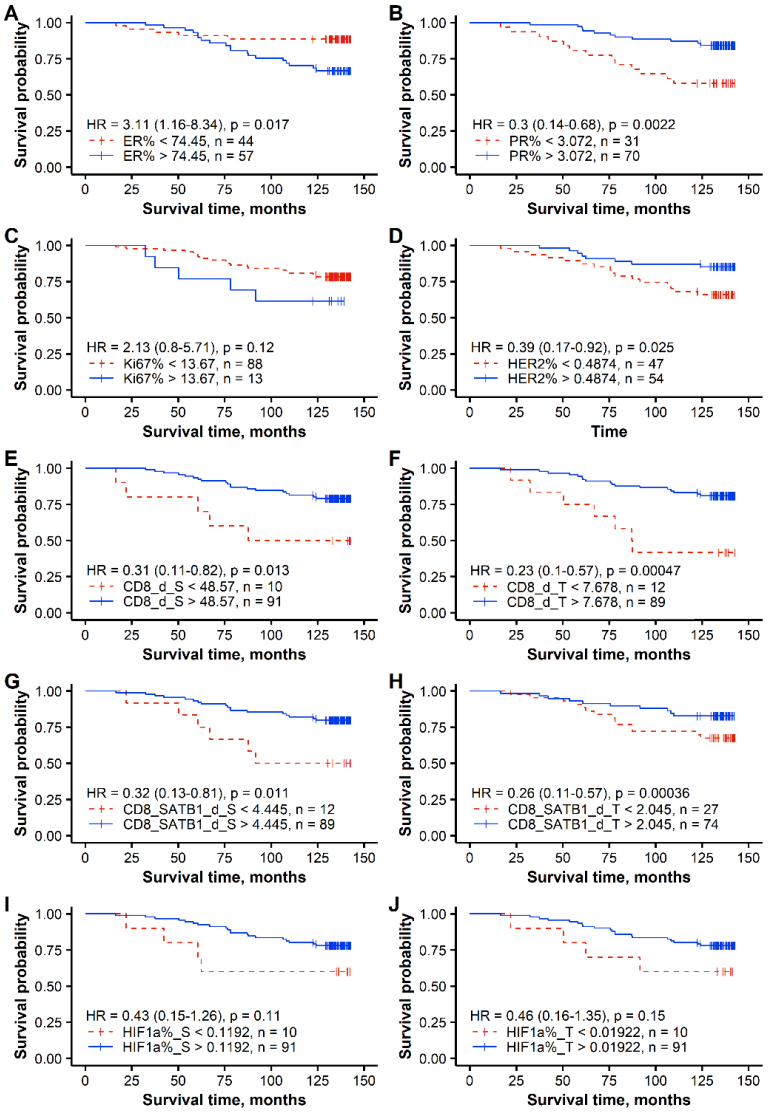

continued on next page

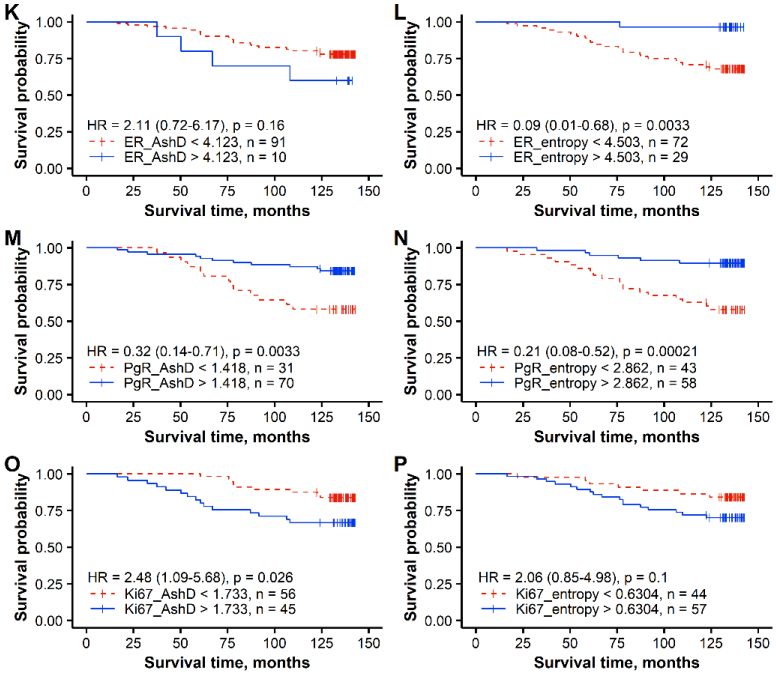

AshD, Ashman's D; d, density; S, stroma; T, tumor.

Figure 6. Kaplan-Meier survival curves with a hazard ratio (HR) and log-rank test for correlation of the immunogradient indicators with overall survival.

The independent prognostic value of the IHC biomarker expression rates, immune response, and intratumoral heterogeneity indicators was tested by multiple Cox regression analysis along with the conventional clinicopathological variables (Table 3). Two prognostic models were investigated: model 1 was produced from the age group, pathology characteristics (pT, pN, and grade), and the conventional BC IHC DIA indicators (percentage of ER, PR, HER2, and Ki67 in the tumor part); while model 2 was obtained by adding the intratumoral heterogeneity and immune response indicators to the data set (Table 3). Model 1 showed the independent prognostic value of two indicators: the higher PR expression predicted a better OS while worse OS was predicted by lymph node involvement.

Meanwhile, model 2 revealed three novel IHC indicators: better OS was predicted by higher CD8+SATB1+ immune cell density in the tumor tissue and higher Haralick's texture entropy of PR; in contrast, worse OS was predicted by the Ki67 AshD bimodality indicator in the tumor tissue. Cox regression models were validated using leave-one-out cross-validation; the frequency of the model 1 and 2 was 58 and 61 times, respectively. Moreover, model 2 showed a remarkable increase in the LR's statistical significance (12.23 compared to 27.67 of model 2).

Table 3. Statistics of multiple Cox regression analyses for correlation of the immunohistochemistry and intratumoral heterogeneity indicators with overall survival:

Indicator	Hazard ratio	95% confidence interval	*p-value*
Model 1, LR: 12.23, $p = 0.0022$			
pN group (pN0 vs. pN1–3)	2.30	1.01–5.28	0.0485
PR%	0.29	0.13–0.66	0.0028
Model 2, LR: 27.67, $p < 0.0001$			
CD8_SATB1_d_T	0.30	0,13–0.67	0.0035
PR_entropy	0.22	0.08–0.56	0.0015
Ki67_AshD	3.26	1.40–7.61	0.0062

AshD, Ashman's D; d, density; T, tumor part; pN, lymph node metastasis status; LR, likelihood ratio.

3.5 Non-linear Relationship Between the Percentage of PR and its Intratumoral Heterogeneity

A non-linear association between the percentage of PR and its intratumoral heterogeneity was noticed: high Haralick's texture entropy of PR was detected within the range from 20 to 80% of PR (Figure 7). Neither of these two indicators was associated with other clinicopathological characteristics.

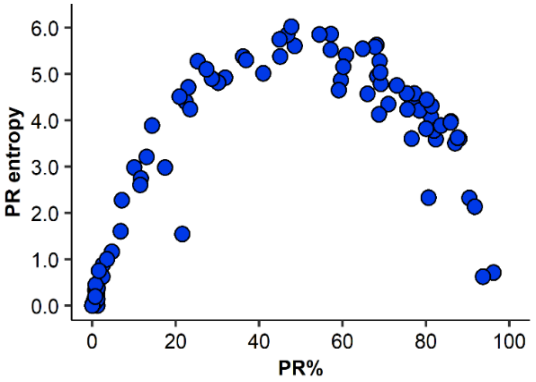

Figure 7. Non-linear association between the percentage of progesterone receptor (PR) and its intratumoral heterogeneity (Haralick's texture entropy).

3.6 Non-linear Relationship Between the Percentage of PR and its Intratumoral Heterogeneity

To explore the prognostic impact of the non-linear relationship between the percentage of PR and its intratumoral heterogeneity, the patients were stratified into three groups:

1) low PR expression rate (<20%) with low Haralick's texture entropy of PR,

2) moderate PR expression rate (20–80%) with high Haralick's texture entropy of PR,

3) high PR expression rate (higher than 80%) with low Haralick's texture entropy of PR.

Patients with a 20–80% expression rate of PR were associated with the best OS (91% OS probability after 143 months), followed by >80% (71% OS) and <20% expression rate of PR (63% OS) (Figure 8).

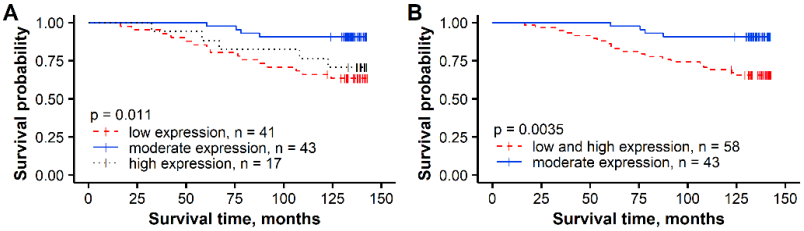

(A) Kaplan-Meier survival curves analyzing low (<20%), moderate (20–80%), and high (>80%) expression rate of PR. (B) Kaplan-Meier survival curves analyzing low and high (<20% and >80%) and moderate (20–80%) expression rate of PR.

Figure 8. Kaplan-Meier survival curves with a hazard ratio (HR) and log-rank test for correlation of the percentage of progesterone receptor with overall survival.

4. DISCUSSION

4.1 Extraction of TE and IZ

After applying automated extraction of the tumor-stroma IZ, density profiles of TIL and novel immunogradient indicators to describe an antitumor immune response were calculated. Although in this work the IZ was defined similarly to the concept of IM used in pathology and other DIA studies [22, 25, 26, 67-69], the tumor-stoma IZ was determined in a completely automated way, based only on DIA data without any visual assessment. Moreover, the IZ was determined by intervals that enabled the calculation of immune cell density indicators across the IZ to reflect the immune cells' gradient from stroma to tumor side and also provided a possibility to adjust TE and IZ's width and spatial positioning of the stroma, TE, and tumor aspects within the IZ.

In several recent studies [28, 34], DIA with mathematical modeling was also used to automatically determine tumor and stroma regions and calculate TME indicators. Harder et al. [28] performed a comprehensive analysis of the immune contexture to determine disease recurrence by applying tissue phenomics methodology in 90 patients with prostate cancer. They automatically determined the boundary between tumor and stroma based on the tumor's morphological features, cytokeratin 18, and p63 IHC data and distinguished 112.5 and 225 μm broad TME zones. Subsequently, they calculated the density and distance indicators of CD3+, CD8+, CD34+, CD68+, and CD163+ cells and determined that a statistically significant prognosis can be made according to the CD8+ and CD34+ ratio within the detected zones. However, the gradient properties of immune response were not investigated in this prostate cancer cohort. In the meantime, the spatial aspects of CD8+ cells infiltration were evaluated by Li et al. [34] in 28 patients with triple-negative BC. Although these scientists used pan-cytokeratin fluorescent staining to delineate the tumor-stroma boundary

manually, they used the DIA algorithm to expand it to the 500 μm fixed-width IM. Despite this manual step, CD8+ cell pixels and TIL mobility were evaluated across the boundary and determined that chemokines prevent T lymphocytes from entering the tumor's core. In both studies, the tumor-stroma region was determined not according to the classic definition of IM but similar to the method used in this dissertation. However, according to this work's strategy, IZ extraction was less dependent on the type of tumor growth pattern and did not require any additional IHC staining. On the other hand, IZ was not determined as a fixed-width boundary; it precisely reflected three-dimensional interfaces of tumor and stroma elements and their spatial aspects in two-dimensional pathology slides. Therefore, the applied methodology was less dependent on the tumor's specific morphological features, more sensitive and precise than other the abovementioned comparable automatic or semiautomatic methods to determine IM.

4.2 Association between Immunogradient Indicators and Survival Data

After automated TE and IZ extraction, the prognostic value of quantitative and directional variance variables of CD8+ immune cells was explored and enabled independent prognostic stratification of HRBC patients (Table 2 and Figure 5). It was determined that quantitative CD8+ cell density indicators have prognostic value in the early-stage HRBC cohort. For example, the mean of CD8+ cell density in the tumor aspect of IZ_9 was related to a better prognosis. Moreover, in the multiple Cox regression model, it was found that the mean of CD8+ cells density within the tumor aspect of IZ_9 is a strong and independent indicator of the better OS in the context of age, pN status, and CM for CD8+ density by mean (Table 2, model 1). Remarkably, it was found that indicators that reflected the spatial distribution of CD8+ cells within the IZ were independent predictors of better OS. The CM indicator, which reflected the gradient of

CD8+ cells toward the IZ tumor part, was also related to better survival in the HRBC patient cohort and was an independent indicator in the multiple Cox regression model (Table 2, model 1). Respectively, it was detected that the ID indicator, which reflected an abrupt decrease of CD8+ cell density in the IZ tumor aspect, is associated with a shorter patient survival time. This parameter was only one variable from the set of immunogradient indicators that did not depend on IZ's width and could be calculated in the narrowest IZ (IZ_3). This aspect also raised the hypothesis that ID indicator can provide additional prognostic value, especially when tumor aspect ranking can be limited, for example, in biopsy material or when tumor tissue content is low. It was also noticed that spatial distribution indicators provide more prognostic information than CD8+ cell density indicators (Table 2, model 1 and 2).

The factor analysis of IZ CD8+ density variables revealed two orthogonally independent factors of variation: CD8+ cell density level (factor 1) and CD8+ density gradient factor (factor 2), which were significantly associated with better OS in univariate analyses (Figure 5, J and K). Furthermore, in the multiple Cox regression model, it was determined that the aggregated IZ CD8+ factor, calculated by the sum of the CD8+ density and CD8+ gradient factors scores, was an independent prognostic indicator of a longer OS in early-stage HRBC (Table 2, model 2). This result indicated that by combining the absolute density and spatial aspects of immune cells, the TME might be evaluated more precisely, and the additional prognostic value of immune response indicators could be extracted.

Various studies [70-73] have demonstrated the clinical relevance of TIL and detected a positive association with OS in ER-negative, HER2-positive, and triple-negative BC; however, contradicting results have been reported in ER-positive and HER2-negative BC [31, 74]. Meantime, a large-scale study [74] that included 12 439 BC samples found no association between the survival and visually quantified cytotoxic T cells. Nevertheless,

in ER-positive BC, Sobral-Leite et al. [31], based on IHC and DIA data, detected that CD8+ T cells' density was associated with worse prognosis and mutations of the *PIK3CA*. On the other hand, Lee and colleagues [75] indicated that the relevance of TIL could have a different prognostic effect on different BC subtypes; however, their results were not statistically significant. Despite that, in this thesis, based on IHC and DIA, the prognostic value of immunogradient indicators were retrieved. Remarkably, a time-dependent effect was determined by analyzing the relationship between aggregated IZ CD8+ factor and survival in the early-stage HRDK cohort – more than 92% of patients survived 5 years after surgery. In contrast, after 5 years, patients' survival probability started to differ significantly; after 10 years, the survival probability between high and low indicator groups differed by 32% (Figure 5, L). This result emphasizes that the antitumor immune response might be detected by the methodology described in this thesis and that the aggregated IZ CD8+ factor can determine the long-term prognosis for patients with a relatively well-controlled disease.

4.3 Association between IHC Biomarkers and Survival Data

Besides, an integrated IHC image-based biomarker data set was created to explore the interactions of cancer and immune cells and their clinical value in the HRBC microenvironment. The multidimensional model achieved from clinicopathological parameters, conventional BC biomarkers (ER, PR, HER2, and Ki67), immune response, hypoxia-inducible, and intratumoral heterogeneity indicators demonstrated that the prognostic modeling is possible in HRBC patients based entirely on the DIA results. This model reflected three new biological features of HRBC – PR expression,

the intensity of proliferation, and immune response (Table 3, model 2). It is worth to notice that these indicators surpassed standard clinical and pathological parameters in the tested dataset. Moreover, it was also determined that the intratumoral heterogeneity parameters of PR and Ki67 expression provide more prognostic information than the quantitative estimates of their expression, while the use of Haralick's texture and bimodality indicators to describe the intratumoral heterogeneity of biomarkers' expression can significantly increase the statistical power of the prognostic model (Table 3, model 1 and 2). It was also proved that intratumoral heterogeneity of PR and density of CD8+SATB1+ cells in tumor compartment are independent indicators of better prognosis in early-stage HRBC (HR = 0.22, p = 0.0015 and HR = 0.3, p = 0.0035, respectively) and provided new data insights into BC's biological processes.

4.3.1 Association between Immune Response indicators and Survival Data

In the literature [76-80], it has been shown that SATB1 is related to the aggressive phenotype and worse patient prognosis; however, this protein's clinical and prognostic significance in various malignancies remains controversial. In particular, Cai et al. [81] and Han et al. [76] determined that an excessively high expression of SATB1 is associated with the aggressiveness of BC; however, Iorns et al. [82] have not found an association between higher SATB1 transcript level and BC's pathogenesis. In contrast, Selinger et al. [83] determined that a decrease of SATB1 is related to a worse prognosis in lung squamous cell carcinoma. These discrepancies could have been caused by the fact that many studies [76, 82, 84, 85] that include SATB1 in the analysis of pathogenesis were carried out in tumor extracts without distinguishing different tissue parts. This aspect is essential, because gene expression studies [86-88] confirmed that SATB1 regulates around 300 T cells' genes, while other studies [88, 89] have

indicated that mice without SATB1 expression in lymphocytes die, on average, after three weeks due to immune system disorders. Moreover, in 2017, Stephen et al. [90] have demonstrated in mouse models that the decreased expression of SATB1 in T cells leads to a 40-times increased programmed cell death protein 1 (PD1) synthesis that disturbs the immune cells' proliferative capacity and effector functions. These results suggest that previous studies [76, 82, 84, 85] that analyzed SATB1 at the molecular level without separating the tumor and TME cells could be inaccurate. Therefore, in this study, the expression of SATB1 was evaluated not only in separate parts of tumor tissue but also by examining the origin of cytotoxic T cells.

Double IHC for SATB1 and CD8 proteins was applied to evaluate the changes of expression of SATB1 in tumor and immune cells. DIA results on whole slide images demonstrated that a higher expression of SATB1 is prognostically essential and confirmed a previous study's [91] findings based on TMA in the same patient cohort. However, by exploring the CD8 expression in one slide with SATB1, it was proved that the prognostic value of this protein is related to the density of CD8+SATB1+ cells in the tumor compartment (Table 3, model 2). On the other hand, the CD8+ density in the tumor part was also related to a better prognosis (HR = 0.23, $p = 0.00047$); however, in the multiple Cox regression model, it was outperformed by the tumoral CD8+SATB1+ density (HR = 0.3, $p = 0.0035$). According to these results, it was determined that CD8+SATB1+ T cells provide more prognostic information than the assessment of CD8+ lymphocytes and supported the hypothesis that SATB1 in CD8+ T cells reflects the feature of activated cytotoxic immune cells and may serve as a potential immune response biomarker in malignancies.

4.3.2 Association between Conventional BC Biomarkers and Survival Data

IHC assessment of ER and PR expression has been already used for a few decades to determine BC patient's prognosis and response to hormone therapy [92]. In clinical practice, IHC results are evaluated using qualitative status and subsequently assigned to negative, weakly positive, or positive tumors; however, studies [92-95] have proved that quantitative assessment of ER and PR expression could provide additional prognostic value. For example, Barllet et al. [93] determined that an ER and PR IHC quantitative assessment allows predicting the risk of early disease reoccurrence for patients diagnosed with moderate hormone receptor expression compared to the high expression group (>80–85% of ER and >75% of PR) and demonstrated that patients with a high rate of ER might get additional benefit from exemestane [93]. After applying DIA and a quantitative assessment of ER and PR in this work, it was also found that a higher than 74% expression of ER was associated with a worse prognosis, while a higher than 3% expression of PR predicted better OS. Moreover, the multiple Cox regression model composed of clinicopathological features and conventional BC biomarkers allowed to determine the independent prognostic value of PR expression (HR = 0.29, p = 0.0028) in the context of lymph node involvement (Table 3, model 1). Similar results were provided by Purdie et al. [96] in the study of 1 283 patients with early-stage BC. They found that PR's higher expression is an independent indicator of better prognosis in the context of pT and pN status, grade, and expression of ER. Despite that, a recent meta-analysis [92] of 19 studies, which consisted of 30 754 BC samples, demonstrated that there is no clear evidence that the quantitative assessment of ER and/or PR could provide prognostic or predictive data. However, they proposed in pathology reports no longer provide hormone receptor expression's qualitative status to prevent oncologists unconsciously making different treatment decisions [92]. In addition to

that, in 2020, the American Society of Clinical Oncology and the College of American Pathologists recommended cases with low expression of ER (1–10%) report with the additional comment that the biological aspect of this type of tumors is more similar to ER-negative cases and that hormone therapy might not add any benefit [9]. However, these guidelines did not provide a strategy for ensuring accurate and reproducible results for IHC assessment.

4.3.3 Association between Intratumoral Heterogeneity and Survival Data

Based on the hexagonal grid tiling methodology developed previously for the Ki67 heterogeneity assessment [44-46], ER, PR, and Ki67 Haralick's texture and AshD bimodality indicators were calculated in this work. An analysis of PR heterogeneity revealed a non-linear relationship between the intensity of PR expression rate and PR Haralick's texture entropy in the tumor tissue (Figure 7). This finding was also reported previously for Ki67 and was explained by the extracted features' nature – lower heterogeneity is found in samples with a low or high expression rate [44]. However, in the multiple Cox regression model, it was found that the PR entropy is an independent indicator of better OS, which outperformed a quantitative assessment of PR expression rate (Table 3, model 2). This result highlighted the importance of the detected association and was confirmed by dividing patients into three groups according to intensity of expression rate: worse OS prognosis was detected for patients who were assigned to low (<20%) and high (>80%) expression rate of PR compared to patients with moderate expression of PR (>20% but <80%) (p = 0,0035) (Figure 8, B). The biological meaning of this non-linear relationship between PR expression and its entropy should be analyzed more thoroughly; however, it confirms the notion that “intratumor heterogeneity is universal, although perhaps non-linear prognostic biomarker” [97]. This result may also explain why the previous efforts to quantify hormone

receptors to determine prognostic and/or predictive value were controversial [92-96].

The independent prognostic value of Ki67 intratumoral heterogeneity, measured by the AshD indicator, was also determined in this work (Table 3, model 2). In the multiple Cox regression model, the Ki67 bimodality indicator outperformed the Ki67 expression rate *per se* and was related to a worse prognosis. This result was achieved on a different patient cohort, in different laboratory stained IHC slides and applying different DIA (different tissue classifier) and parameters of hexagonal tiling methodology (different side length of hexagons); however, it replicated the previous study's finding [44] and confirmed the prognostic value of Ki67 AshD in BC samples. Additionally, the Ki67 bimodality indicator's independent prognostic value was confirmed in the context of PR heterogeneity and immune response included in this work with early-stage HRBC.

In conclusion, this thesis demonstrates the potential of the fully automated and data-driven methodology to extract tumor-stroma IZ and prognostic value of novel immune response indicators. The immunogradient parameters allowed dichotomizing patients into worse and better prognosis groups and revealed prominent OS probability divergence 5 years after the surgery. On the other hand, an integrated digital IHC prognostic model determined three independent biological features of early-stage HRBC – PR expression, tumor proliferation, and immune response, which outperformed BC's clinical and pathological features. It was also proved that PR and Ki67 heterogeneity indicators provided more prognostic information than its expression rate – high intratumoral heterogeneity for PR and low for Ki67 were determined as independent indicators of longer OS for patients with HRBC. This work also demonstrated that the prognostic effect of SATB1 is related to the intratumoral density of CD8+SATB1+ cells, which could be used as a specific biomarker of antitumor immunity.

CONCLUSIONS

1. IHC procedures were developed and optimized to fit DIA needs for multiparametric and spatial analysis of ER, PR, HER2, Ki67, CD8, and HIF1α expression.
2. The DIA and hexagonal grid subsampling-based IZ detection method automatically extracts the tumor-stroma IZ. It measures the CD8+ density profiles based on immunogradient indicators to assess antitumor immune response across the IZ.
3. The aggregated IZ CD8+ cell response factor is an independent indicator of the better OS, which determines the long-term (>5 years) prognosis for patients with HRBC (87% and 55% survival probability after 10 years for high and low indicator groups, respectively).
4. The multidimensional digital IHC prognostic model determined three independent biological features of early-stage HRBC – immune response, heterogeneity of PR expression, and tumor proliferation heterogeneity. This model allows a reliable and independent assessment of prognosis in HRBC patients and outperforms conventional BC IHC and clinicopathological features.
5. Intratumoral CD8+SATB1+ cell density (>2 cells/mm^2) is an independent predictor of improved OS in the HRBC cohort and could potentially serve as a specific biomarker of antitumor immunity.

LIST OF PUBLICATIONS

Publications:

1. Rasmusson A, **Zilenaite D**, Nestarenkaite A, Augulis R, Laurinaviciene A, Ostapenko V, Poskus T, Laurinavicius A. Immunogradient indicators for anti-tumor response assessment by automated tumor-stroma interface zone detection. Am J Pathol. 2020;190(6):1309-1322.
2. **Zilenaite D**, A. Rasmusson A, Augulis R, Besusparis J, Laurinaviciene A, Plancoulaine B, Ostapenko V, Laurinavicius A. Independent Prognostic Value of Intratumoural Heterogeneity and Immune Response Features by Automated Digital Immunohistochemistry Analysis in Early Hormone Receptor-Positive Breast Carcinoma. Front Oncol. 2020;10:950.

Patent:

1. Rasmusson A, **Zilenaite D**, Nestarenkaite A, Augulis R, Laurinavicius A. Automated Tumour-Stroma Interface Zone Detection for Anti-Tumour Response Assessment by Immunogradient Indicators. Lithuanian patent application: LT2019 509. PCT patent application: PCT/IB2020/053396. Applicant: Vilnius University (Lithuania).

SUMMARY IN LITHUANIAN

Įvadas

Navikų biologijos tyrimų pažanga ne tik leido suprasti naviko karcinogenezės ir vystymosi procesus, bet ir suteikė pagrindą personalizuotoms terapijoms, kurių didžioji dalis yra nukreiptos prieš naviko ląsteles[10]. Vis dėlto šių terapijų klinikinį naudingumą riboja didelis naviko ląstelių populiacijų heterogeniškumas ir netolydus pasiskirstymas individualiame navike[11]. Pastarųjų metų tyrimai[12–16] atskleidė, kad naviko mikroaplinka yra kur kas svarbesnė, negu buvo manyta iki šiol, – ji dalyvauja ląstelių epiteliniame ir mezenchiminiame virsme, skatina angiogenezę, naviko ląstelių išplitimą, imuninę infiltraciją, o išreguliuotas imuninis atsakas ir ląstelių tarpusavio sąveikos skatina naviko progresiją ir terapijos atsparumą, taip veikdamos naviko gydymą ir prognozę. Taigi, galima teigti, kad naviko mikroaplinka yra kritinė naviko ląstelių „partnerė“[98], ir kelti hipotezę, kad išsami naviko ląstelių ir mikroaplinkos profilių analizė naviko erdviniame kontekste gali atskleisti tarp naviko ir imuninės sistemos komponentų vykstančių sąveikų dinamiką bei suteikti ne tik prognozinę, bet ir predikcinę vertę. Vienas iš svarbiausių naviko mikroaplinkos elementų – naviką infiltruojantys limfocitai (NIL). Apie šių limfocitų įtaką pacientų prognozei žinoma jau nuo XIX a.[17, 18], tačiau tik neseniai atlikti išsamūs tyrimai, įrodantys NIL klinikinę reikšmę[19–21].

Storosios žarnos navikų imunohistocheminiai (IHC) ir skaitmeninės vaizdo analizės (SVA) imuninių ląstelių tyrimai[20] leido nustatyti, kad NIL sudėtis, ypač CD8+ ir CD3+ T ląstelės, tankis ir jų pasiskirstymas naviko audinyje (centre arba periferijoje), turi didelę prognozinę vertę. Nepaisant to, tiriant krūties vėžį (KV), NIL įvertinimas iki šiol nėra įdiegtas į kasdienę klinikinę praktiką[24–26], nors Tarptautinė imunoonkologinių biožymenų darbo grupė NIL įvertinimo rekomendacijas pateikė dar 2017 m.[25, 26]. Remiantis šiomis gairėmis, NIL tyrimas turėtų būti atliekamas hematoksilinu ir

eozinu dažytuose mėginiuose pusiau kiekybiniu būdu, nustatant erdvinius aspektus – 1 mm pločio invazijos kraštą (IK), kuris skiria navikinį audinį nuo aplinkinio stromos komponento[25–27]. Rekomendacijomis siekta suvienodinti NIL tyrimus įvairiuose navikuose, tačiau, analizuojant naviko mikroaplinką pagal šias gaires, nėra galimybės įvertinti imuninių ląstelių sudėtį, kiekybinis ir erdvinis įvertinimas yra subjektyvus ir labai priklauso nuo vertintojo patirties. Dėl minėtų priežasčių, atliekant tyrimus[20, 21, 28–31], pasiūlyta taikyti IHC metodą, kuris leidžia ne tik nustatyti imuninio komponento fenotipą, bet ir apibūdinti naviką dvimatėje erdvėje. Taip gaunama daugiau informacijos apie biologines sąveikas naviko mikroaplinkos kontekste. Dviguba IHC šį metodą gali sustiprinti, nes suteikiama galimybė nustatyti ląstelės tipą ir jos biologines savybes[32, 33]. Vis dėlto tyrimai[28, 34], leidžiantys įvertinti erdvinius aspektus – atskirti navikinio audinio regionus ir automatizuotu būdu nustatyti naviko ir stromos sąveikos zoną (SZ), iki šiol yra pavieniai. Gauti prieštaringi rezultatai, vertinant NIL ir KV sergančių pacientų prognozę[29, 35–40], ypač plačiausioje KV grupėje – hormonų receptorių teigiamose duktalinėse karcinomose (HRDK), rodo, kad NIL tyrimas pagal vizualaus įvertinimo mikroskopuojant rekomendacijas nėra pakankamai tikslus. Priešingai, NIL įvertinimas, taikant IHC ir SVA metodus, leistų gauti tikslius kiekybinius parametrus, tokius kaip konkrečių imuninių ląstelių skaičius, paviršiaus plotas ar kiti rodikliai. Be to, taikant šešiakampių gardelių analitiką ir erdvinės statistikos metodus, kai kurių tyrėjų darbuose[44–46] rekomenduotus Ki67 heterogeniškumui įvertinti, būtų galima automatiškai vizualizuoti navikinio audinio komponentus, įvertinti žymenų erdvinį pasiskirstymą, o nustatytus esminius imuninį atsaką apibūdinančius rodiklius susieti su pacientų išgyvenamumo duomenimis.

Nepaisant pažangos matuojant imuninį atsaką, fundamentalus klausimas, kodėl dauguma navikų neturi žymaus imuninio atsako, lieka neatsakytas. Terapijos, paremtos imuninio atsako aktyvinimu, priklauso nuo NIL, tačiau dėl naviko ląstelių sintetinamų įvairių baltymų (pavyzdžiui, 1-ojo užprogramuoto ląstelių mirties baltymo

ligando) naviko imunogeniškumas, nepaisant didelio NIL tankio, gali būti slopinamas[48–50], o kuriamos imunoterapijos mažai efektyvios[51–55]. Dėl šios priežasties išsamūs naviko ląstelių, įskaitant antigenų pateikimo, angiogenezės, proliferacijos bei kitų navikų patogenezės progresijos (naviko dydžio, išplitimo į limfmazgius ir kt.) požymių, imuninio atsako ir naviko erdvinės tekstūros, tyrimai ne tik geriau atskleistų naviko ir mikroaplinkos ląstelių sąveikas, bet ir leistų gauti tikslesnę informaciją apie HRDK pacientų prognozę.

Tyrimo tikslas

Įvertinti krūties vėžio progresijos požymių ir imuninio atsako sąsajas naviko mikroaplinkos erdviniame kontekste.

Darbo uždaviniai

Tikslui įgyvendinti iškelti šie tyrimo uždaviniai:

1. Sukurti viengubos ir dvigubos imunohistochemijos tyrimo metodikas naviko ir jo mikroaplinkos žymenų raiškai įvertinti ir jas pritaikyti kiekybinei bei erdvinei skaitmeninei vaizdo analizei.
2. Sukurti skaitmeninės vaizdo analizės ir šešiakampių gardelių principais paremtą metodologiją krūties vėžio mikroaplinkos komponentams nustatyti, išskirti naviko ir stromos sąveikos zoną ir joje atlikti ląstelių erdvinio pasiskirstymo matavimus.
3. Optimizuoti naviko, jo mikroaplinkos, imuninio atsako ir biožymenų heterogeniškumo rodiklių rinkinius krūties vėžio patobiologiniams ir prognoziniams modeliams kurti.
4. Įvertinti sukurtų rodiklių rinkinių sąsajas su patologijos ir klinikos duomenimis bei prognozine verte pacienčių, sergančių ankstyvosios stadijos hormonų receptorių teigiama duktaline karcinoma, imtyje.

Ginamieji disertacijos teiginiai

1. Sukurta krūties vėžio audinio tyrimo metodologija leidžia automatiškai nustatyti naviko ir stromos sąveikos zoną bei apskaičiuoti antinavikinį imuninį atsaką apibūdinančius imunogradiento rodiklius, kurie leidžia prognozuoti pacienčių, sergančių ankstyvosios stadijos hormonų receptorių teigiama duktaline karcinoma, bendrąjį išgyvenamumą.
2. Skaitmenine vaizdo analize pagrįstas integruotas Ki67, progesterono receptorių (PgR) ir CD8+SATB1+ imunohistochemijos modelis, nepriklausomai nuo klinikos ir patologijos parametrų, leidžia įvertinti pacienčių, sergančių hormonų receptorių teigiama duktaline karcinoma, prognozę. Šis modelis atskleidžia, kad Ki67 ir PgR raiškos vidunavikinio heterogeniškumo rodikliai suteikia daugiau prognozinės informacijos negu šių biožymenų kiekybiniai įverčiai, o CD8+SATB1+ ląstelių tankis navike gali būti taikomas kaip aktyvaus imuninio atsako prieš naviką rodiklis.

Darbo naujumas ir reikšmė

1. *Naviko ir stromos sąveikos krašto (SK) ir SZ nustatymo metodologija*. Pritaikius SVA ir skaitmenizuoto KV audinio padalijimo į šešiakampius gardelių elementus metodus, šiame darbe automatiškai nustatytas naviko ir stromos SK bei SZ. SZ nustatymas intervalais (rangais) leido optimizuoti SZ plotį ir apskaičiuoti kiekybinius ir erdvinius imuninį atsaką apibūdinančius imunogradiento rodiklius ankstyvosios stadijos HRDK mėginiuose.

2. *Imunogradiento rodiklių prognozinė vertė.* Šiame darbe pirmą kartą nustatyta, kad ne tik CD8+ ląstelių tankis naviko dalyje, bet ir šių ląstelių gradientą į naviką apibūdinantis parametras – CD8+ ląstelių tankio masės centras – yra nepriklausomi geros prognozės rodikliai HRDK imtyje. Be to, nustatyta, kad agreguotas SZ CD8+ ląstelių imuninio atsako

faktorius, kuris sujungia kiekybinio ir erdvinio imuninio atsako įvertinimo aspektus, yra nepriklausomas HRDK sergančių pacienčių bendrojo išgyvenamumo rodiklis, ypač vertinant ilgalaikę (>5 m.) prognozę.

3. *CD8+SATB1+ ląstelių biologinė ir prognozinė vertė*. Pritaikius SATB1 ir CD8 dvigubos IHC SVA, pirmą kartą nustatyta, kad plataus masto epigenetinio reguliatoriaus SATB1 prognozinis poveikis HRDK yra susijęs su vidunavikiniu CD8+SATB1+ ląstelių tankiu. Taip pat nustatyta, kad CD8+SATB1+ T ląstelės suteikia daugiau prognozinės informacijos negu kiekybinis CD8+ limfocitų įvertinimas. Tikėtina, kad SATB1 raiška CD8+ ląstelėse atspindi aktyvuotą imuninių ląstelių būklę.

4. *Netiesinis ryšys tarp PgR raiškos intensyvumo ir vidunavikinio heterogeniškumo bei PgR entropijos prognozinė vertė.* Empiriškai įrodyta netiesinė priklausomybė tarp PgR raiškos lygmens ir jo vidunavikinio heterogeniškumo (Haralicko entropijos) pirmą kartą atskleidžia, kad vidutinė (20–80 %) PgR raiška yra susijusi su geresne HRDK prognoze. Be to, PgR heterogeniškumo rodiklio prognozinė vertė yra didesnė negu šio biožymens raiškos kiekybinis įvertis (PgR-teigiamų KV ląstelių dalis).

5. *SVA duomenimis pagrįstas integruotas prognozinis modelis*. Pirmą kartą, remiantis vien tik IHC SVA duomenimis, gautas integruotas prognozinis modelis, kuris pranoko standartinius KV klinikos ir patologijos parametrus bei atspindėjo tris biologiškai svarbius ir savarankiškus HRDK naviko požymius – PgR raiškos, KV proliferacijos intensyvumo ir naviko mikroaplinkos imuninio atsako.

Rezultatų aptarimas

Skaitmenizuotuose mikroskopiniuose patologijos vaizduose, pritaikius automatizuotą naviko ir stromos komponentų atskyrimo

įrankį SK nustatyti ir SZ išskirti, apskaičiuoti imuninių ląstelių tankio profiliai bei nauji kiekybiniai ir erdviniai antinavikinį imuninį atsaką apibūdinantys rodikliai, kurie buvo susieti su pacienčių išgyvenamumo duomenimis. Taikant pasirinktą tyrimo metodą, SZ apibrėžta panašiai kaip ir kituose tyrimuose[22, 25, 26, 67-69], tačiau ji buvo nustatyta visiškai automatizuotai, remiantis tik SVA duomenimis. Be to pagal šio darbo tyrimo strategiją, SZ nustatymas buvo mažiau priklausomas nuo naviko augimo pobūdžio, tikslumo atpažįstant ir segmentuojant atskiras naviko ląsteles ir nereikalavo papildomų IHC dažymų naviko audinio komponentams atskirti. Antra vertus, SZ nebuvo nustatyta kaip fiksuoto pločio riba, o tiksliai atspindėjo trimates naviko ir stromos elementų sąsajas ir jų erdvinius aspektus dvimačiame patologijos vaizde.Taip pat taikant šį tyrimo metodą, SZ buvo nustatyta intervalais, todėl imuninio atsako rodikliai apskaičiuoti taip, kad atspindėtų imuninio infiltrato gradientą nuo stromos į naviką arba kad atspindėtų rodiklių dispersiją konkrečioje SZ dalyje. Nustatytas erdvinis (CD8+ tankio poslinkis į naviko šerdį) ir kiekybinis (absoliutus CD8+ tankis navike) imunogradiento parametrai vertintini kaip nepriklausomi ankstyvosios stadijos HRDK sergančių pacienčių bendrojo išgyvenamumo rodikliai.

Sukurtas HRDK mikroaplinkos ir erdvinio konteksto požymių modelis, kurį sudarė klinikiniai, patologiniai, standartinių KV biožymenų (ER, PgR, HER2 ir Ki67), imuninį atsaką ir hipoksijos savybes apibūdinantys rodikliai, buvo susietas su HRDK pacientų išgyvenamumo parametrais. Šis prognozinis modelis ne tik patvirtino disertacijos pirmos dalies rezultatus, kad HRDK naviko mikroaplinka yra biologiškai ir prognoziškai svarbus elementas, bet ir leido nustatyti, jog integruotas prognozinis modelis gali būti gautas remiantis vien tik IHC mėginių SVA duomenimis ir atspindėti tris biologinius HRDK požymius: PgR raiškos, proliferacijos intensyvumo ir naviko mikroaplinkos imuninio atsako. Reikia pastebėti, kad šie rodikliai pranoko KV standartinius klinikinius ir patologinius parametrus. Be to, nustatyta, kad vidunavikiniai PgR ir Ki67 raiškos heterogeniškumo rodikliai suteikia papildomos

prognozinės vertės, palyginti su šių biožymenų kiekybiniais įverčiais, o pasitelkus Haralicko tekstūros ir bimodališkumo rodiklius vidunavikiniam biožymenų raiškos nevienalytiškumui apibūdinti, galima žymiai padidinti prognozinio modelio statistinį reikšmingumą. Disertacijoje taip pat įrodyta, kad vidunavikinis PgR heterogeniškumas ir CD8+SATB1+ ląstelių tankis navike yra ankstyvosios stadijos HRDK nepriklausomi geros prognozės rodikliai, kurie atkleidžia naujų įžvalgų apie KV biologiją ir heterogeniškumą.

Išvados

1. Sukurtos SVA reikalavimus atitinkančios standartizuotos ER, PgR, HER2, Ki67, CD8 ir HIF1α IHC procedūros.
2. SVA rezultatų šešiakampių gardelių analitika pagrįstas KV audinio mikroaplinkos tyrimo metodas leidžia automatizuotai nustatyti naviko ir stromos SZ ir joje apskaičiuoti CD8+ imuninių ląstelių tankio profilius ir antinavikinį imuninį atsaką apibūdinančius imunogradiento rodiklius.
3. Ankstyvosios stadijos HRDK sergančių pacienčių imtyje nustatyta agreguoto SZ CD8+ imunogradiento faktoriaus nepriklausoma teigiama prognozinė vertė. Šis rodiklis leidžia patikimai prognozuoti atokius (po 5 metų) pacienčių išgyvenamumo duomenis (atitinkamai 87 % ir 55 % išgyvenamumo tikimybės po 10 metų).
4. Sukurtas integruotas IHC biožymenų raiškos vidunavikinio heterogeniškumo ir antinavikinio imuninio atsako modelis, pagrįstas trimis IHC biožymenimis, apibūdinančiais HRDK biologinius požymius: imuninio atsako, PgR raiškos heterogeniškumo ir naviko proliferacijos heterogeniškumo. Šis modelis leidžia patikimai ir nepriklausomai nuo klinikinių ir patologijos parametrų įvertinti HRDK bendrojo išgyvenamumo prognozę. Reikšmingų sąsajų su patologijos, klinikos duomenimis nenustatyta.

5. CD8+SATB1+ ląstelių tankis navike (>2 ląstelės/mm^2) yra nepriklausomas geros HRDK prognozės rodiklis, kuris gali būti vertinamas kaip aktyvaus imuninio atsako prieš naviką požymis.

CURRICULUM VITAE

Vardas, Pavardė	Dovilė Žilėnaitė
Bendra informacija	
Gimimo data	1990 m. spalio mėn. 12 d.
Pagrindinė darbovietė	Medicinos genetikė, Valstybinis patologijos centras, VšĮ Vilniaus universiteto ligoninės Santaros klinikų filialas
Asmeniniai kontaktai	Tel. +370 6 98 39 111, el. paštas: dovilezil@yahoo.com
Išsilavinimas	
2015–2021	Vilniaus universitetas, Medicinos fakultetas, medicinos ir sveikatos mokslų srities doktorantūra
2013–2015	Vilniaus universitetas, Medicinos fakultetas, medicinos genetiko magistras (*Cum laude*)
2009–2013	Vilniaus universitetas, Chemijos fakultetas, biochemijos bakalauras
Konferencijos, kvalifikacijos kėlimas	
2019	Tarptautinė konferencija „31st European Congress of Pathology“ Nicos mieste, Prancūzija
2019	Tarptautinė konferencija „25th Global Meet on Cancer Research & Oncology“ Romos mieste, Italija
2019	Mokslinė-praktinė konferencija „Biomedicininė diagnostika: mokslas ir pratika“
2019	Mokslinių paskaitų ciklas „Research Ethics&Research Integrity: Basics and recent development“
2018	Konferencija „Vėžio diagnostikos ir gydymo aktualijos“
2018	Mokslinė-praktinė konferencija „Šiuolaikinės krūties vėžio gydymo tendencijos"

2017	*Milestone* įmonės organizuoti kvalifikacijos kėlimo kursai *Papa Giovanni* XXIII ligoninėje, Bergamo miestas, Italija
	Darbo patirtis
Nuo 2015	Medicinos genetikė, Valstybinis patologijos centras, VšĮ Vilniaus universiteto ligoninės Santaros klinikų filialas
2020–2021	Tyrimų asistentė, Rygos Stradinio universitetas, Ryga, Latvija
2019–2021	Jaunesnioji asistentė, Vilniaus universiteto Medicinos fakulteto Patologijos, teismo medicinos ir farmakologijos katedra

REFERENCES

[1] Harbeck N, Gnant M: Breast cancer. Lancet 2017, 389:1134-50.

[2] Harbeck N, Penault-Llorca F, Cortes J, Gnant M, Houssami N, Poortmans P, Ruddy K, Tsang J, Cardoso F: Breast cancer. Nat Rev Dis Primers 2019, 5:66.

[3] Boyle D, McCourt C, Matchett K, Salto-Tellez M: Molecular and clinicopathological markers of prognosis in breast cancer. Expert review of molecular diagnostics 2013, 13:481-98.

[4] Ginsburg O, Bray F, Coleman MP, Vanderpuye V, Eniu A, Kotha SR, Sarker M, Huong TT, Allemani C, Dvaladze A, Gralow J, Yeates K, Taylor C, Oomman N, Krishnan S, Sullivan R, Kombe D, Blas MM, Parham G, Kassami N, Conteh L: The global burden of women's cancers: a grand challenge in global health. Lancet 2017, 389:847-60.

[5] Bray F, Ferlay J, Soerjomataram I, Siegel RL, Torre LA, Jemal A: Global cancer statistics 2018: GLOBOCAN estimates of incidence and mortality worldwide for 36 cancers in 185 countries. CA Cancer J Clin 2018, 68:394-424.

[6] International Agency for Research on Cancer. Global cancer observatory - cancer fact sheets.

[7] Sawaki M, Shien T, Iwata H: TNM classification of malignant tumors (Breast Cancer Study Group). Jpn J Clin Oncol 2019, 49:228-31.

[8] Cserni G, Chmielik E, Cserni B, Tot T: The new TNM-based staging of breast cancer. Virchows Arch 2018, 472:697-703.

[9] Allison KH, Hammond MEH, Dowsett M, McKernin SE, Carey LA, Fitzgibbons PL, Hayes DF, Lakhani SR, Chavez-MacGregor M, Perlmutter J, Perou CM, Regan MM, Rimm DL, Symmans WF, Torlakovic EE, Varella L, Viale G, Weisberg TF, McShane LM, Wolff AC: Estrogen and Progesterone Receptor Testing in Breast Cancer: ASCO/CAP Guideline Update. J Clin Oncol 2020:Jco1902309.

[10] Duffy MJ, Crown J: Companion Biomarkers: Paving the Pathway to Personalized Treatment for Cancer. Clinical Chemistry 2013, 59:1447-56.

[11] Longo DL: Tumor heterogeneity and personalized medicine. The New England journal of medicine 2012, 366:956-7.

[12] Nagarsheth N, Wicha MS, Zou W: Chemokines in the cancer microenvironment and their relevance in cancer immunotherapy. Nat Rev Immunol 2017, 17:559-72.
[13] Woo SR, Corrales L, Gajewski TF: Innate immune recognition of cancer. Annu Rev Immunol 2015, 33:445-74.
[14] Taniguchi K, Karin M: NF-κB, inflammation, immunity and cancer: coming of age. Nat Rev Immunol 2018, 18:309-24.
[15] Disis ML: Immune regulation of cancer. J Clin Oncol 2010, 28:4531-8.
[16] Erin N, Grahovac J, Brozovic A, Efferth T: Tumor microenvironment and epithelial mesenchymal transition as targets to overcome tumor multidrug resistance. Drug Resistance Updates 2020, 53:100715.
[17] Adams JL, Smothers J, Srinivasan R, Hoos A: Big opportunities for small molecules in immuno-oncology. Nature reviews Drug discovery 2015, 14:603-22.
[18] Pandya PH, Murray ME, Pollok KE, Renbarger JL: The Immune System in Cancer Pathogenesis: Potential Therapeutic Approaches. Journal of immunology research 2016, 2016:4273943-.
[19] Galon J, Mlecnik B, Bindea G, Angell HK, Berger A, Lagorce C, Lugli A, Zlobec I, Hartmann A, Bifulco C, Nagtegaal ID, Palmqvist R, Masucci GV, Botti G, Tatangelo F, Delrio P, Maio M, Laghi L, Grizzi F, Asslaber M, D'Arrigo C, Vidal-Vanaclocha F, Zavadova E, Chouchane L, Ohashi PS, Hafezi-Bakhtiari S, Wouters BG, Roehrl M, Nguyen L, Kawakami Y, Hazama S, Okuno K, Ogino S, Gibbs P, Waring P, Sato N, Torigoe T, Itoh K, Patel PS, Shukla SN, Wang Y, Kopetz S, Sinicrope FA, Scripcariu V, Ascierto PA, Marincola FM, Fox BA, Pagès F: Towards the introduction of the 'Immunoscore' in the classification of malignant tumours. J Pathol 2014, 232:199-209.
[20] Galon J, Pagès F, Marincola FM, Angell HK, Thurin M, Lugli A, Zlobec I, Berger A, Bifulco C, Botti G, Tatangelo F, Britten CM, Kreiter S, Chouchane L, Delrio P, Arndt H, Asslaber M, Maio M, Masucci GV, Mihm M, Vidal-Vanaclocha F, Allison JP, Gnjatic S, Hakansson L, Huber C, Singh-Jasuja H, Ottensmeier C, Zwierzina H, Laghi L, Grizzi F, Ohashi PS, Shaw PA, Clarke BA, Wouters BG, Kawakami Y, Hazama S, Okuno K, Wang E, O'Donnell-Tormey J, Lagorce C, Pawelec G, Nishimura MI,

Hawkins R, Lapointe R, Lundqvist A, Khleif SN, Ogino S, Gibbs P, Waring P, Sato N, Torigoe T, Itoh K, Patel PS, Shukla SN, Palmqvist R, Nagtegaal ID, Wang Y, D'Arrigo C, Kopetz S, Sinicrope FA, Trinchieri G, Gajewski TF, Ascierto PA, Fox BA: Cancer classification using the Immunoscore: a worldwide task force. J Transl Med 2012, 10:205.

[21] Pagès F, Berger A, Camus M, Sanchez-Cabo F, Costes A, Molidor R, Mlecnik B, Kirilovsky A, Nilsson M, Damotte D, Meatchi T, Bruneval P, Cugnenc PH, Trajanoski Z, Fridman WH, Galon J: Effector memory T cells, early metastasis, and survival in colorectal cancer. The New England journal of medicine 2005, 353:2654-66.

[22] Galon J, Costes A, Sanchez-Cabo F, Kirilovsky A, Mlecnik B, Lagorce-Pages C, Tosolini M, Camus M, Berger A, Wind P, Zinzindohoue F, Bruneval P, Cugnenc PH, Trajanoski Z, Fridman WH, Pages F: Type, density, and location of immune cells within human colorectal tumors predict clinical outcome. Science 2006, 313:1960-4.

[23] Mlecnik B, Tosolini M, Kirilovsky A, Berger A, Bindea G, Meatchi T, Bruneval P, Trajanoski Z, Fridman WH, Pagès F, Galon J: Histopathologic-based prognostic factors of colorectal cancers are associated with the state of the local immune reaction. J Clin Oncol 2011, 29:610-8.

[24] Salgado R, Denkert C, Demaria S, Sirtaine N, Klauschen F, Pruneri G, Wienert S, Van den Eynden G, Baehner FL, Penault-Llorca F, Perez EA, Thompson EA, Symmans WF, Richardson AL, Brock J, Criscitiello C, Bailey H, Ignatiadis M, Floris G, Sparano J, Kos Z, Nielsen T, Rimm DL, Allison KH, Reis-Filho JS, Loibl S, Sotiriou C, Viale G, Badve S, Adams S, Willard-Gallo K, Loi S: The evaluation of tumor-infiltrating lymphocytes (TILs) in breast cancer: recommendations by an International TILs Working Group 2014. Ann Oncol 2015, 26:259-71.

[25] Hendry S, Salgado R, Gevaert T, Russell PA, John T, Thapa B, Christie M, van de Vijver K, Estrada MV, Gonzalez-Ericsson PI, Sanders M, Solomon B, Solinas C, Van den Eynden G, Allory Y, Preusser M, Hainfellner J, Pruneri G, Vingiani A, Demaria S, Symmans F, Nuciforo P, Comerma L, Thompson EA, Lakhani S, Kim SR, Schnitt S, Colpaert C, Sotiriou C, Scherer SJ, Ignatiadis M, Badve S, Pierce RH, Viale G, Sirtaine N, Penault-Llorca F,

Sugie T, Fineberg S, Paik S, Srinivasan A, Richardson A, Wang Y, Chmielik E, Brock J, Johnson DB, Balko J, Wienert S, Bossuyt V, Michiels S, Ternes N, Burchardi N, Luen SJ, Savas P, Klauschen F, Watson PH, Nelson BH, Criscitiello C, O'Toole S, Larsimont D, de Wind R, Curigliano G, Andre F, Lacroix-Triki M, van de Vijver M, Rojo F, Floris G, Bedri S, Sparano J, Rimm D, Nielsen T, Kos Z, Hewitt S, Singh B, Farshid G, Loibl S, Allison KH, Tung N, Adams S, Willard-Gallo K, Horlings HM, Gandhi L, Moreira A, Hirsch F, Dieci MV, Urbanowicz M, Brcic I, Korski K, Gaire F, Koeppen H, Lo A, Giltnane J, Rebelatto MC, Steele KE, Zha J, Emancipator K, Juco JW, Denkert C, Reis-Filho J, Loi S, Fox SB: Assessing Tumor-infiltrating Lymphocytes in Solid Tumors: A Practical Review for Pathologists and Proposal for a Standardized Method From the International Immunooncology Biomarkers Working Group: Part 1: Assessing the Host Immune Response, TILs in Invasive Breast Carcinoma and Ductal Carcinoma In Situ, Metastatic Tumor Deposits and Areas for Further Research. Adv Anat Pathol 2017, 24:235-51.

[26] Hendry S, Salgado R, Gevaert T, Russell PA, John T, Thapa B, Christie M, van de Vijver K, Estrada MV, Gonzalez-Ericsson PI, Sanders M, Solomon B, Solinas C, Van den Eynden GGGM, Allory Y, Preusser M, Hainfellner J, Pruneri G, Vingiani A, Demaria S, Symmans F, Nuciforo P, Comerma L, Thompson EA, Lakhani S, Kim S-R, Schnitt S, Colpaert C, Sotiriou C, Scherer SJ, Ignatiadis M, Badve S, Pierce RH, Viale G, Sirtaine N, Penault-Llorca F, Sugie T, Fineberg S, Paik S, Srinivasan A, Richardson A, Wang Y, Chmielik E, Brock J, Johnson DB, Balko J, Wienert S, Bossuyt V, Michiels S, Ternes N, Burchardi N, Luen SJ, Savas P, Klauschen F, Watson PH, Nelson BH, Criscitiello C, O'Toole S, Larsimont D, de Wind R, Curigliano G, André F, Lacroix-Triki M, van de Vijver M, Rojo F, Floris G, Bedri S, Sparano J, Rimm D, Nielsen T, Kos Z, Hewitt S, Singh B, Farshid G, Loibl S, Allison KH, Tung N, Adams S, Willard-Gallo K, Horlings HM, Gandhi L, Moreira A, Hirsch F, Dieci MV, Urbanowicz M, Brcic I, Korski K, Gaire F, Koeppen H, Lo A, Giltnane J, Rebelatto MC, Steele KE, Zha J, Emancipator K, Juco JW, Denkert C, Reis-Filho J, Loi S, Fox SB: Assessing Tumor-Infiltrating Lymphocytes in Solid Tumors: A Practical

Review for Pathologists and Proposal for a Standardized Method from the International Immuno-Oncology Biomarkers Working Group: Part 2: TILs in Melanoma, Gastrointestinal Tract Carcinomas, Non-Small Cell Lung Carcinoma and Mesothelioma, Endometrial and Ovarian Carcinomas, Squamous Cell Carcinoma of the Head and Neck, Genitourinary Carcinomas, and Primary Brain Tumors. Advances in anatomic pathology 2017, 24:311-35.

[27] Mlecnik B, Bindea G, Kirilovsky A, Angell HK, Obenauf AC, Tosolini M, Church SE, Maby P, Vasaturo A, Angelova M, Fredriksen T, Mauger S, Waldner M, Berger A, Speicher MR, Pagès F, Valge-Archer V, Galon J: The tumor microenvironment and Immunoscore are critical determinants of dissemination to distant metastasis. Sci Transl Med 2016, 8:327ra26.

[28] Harder N, Athelogou M, Hessel H, Brieu N, Yigitsoy M, Zimmermann J, Baatz M, Buchner A, Stief CG, Kirchner T, Binnig G, Schmidt G, Huss R: Tissue Phenomics for prognostic biomarker discovery in low- and intermediate-risk prostate cancer. Sci Rep 2018, 8:4470.

[29] Liu S, Lachapelle J, Leung S, Gao D, Foulkes WD, Nielsen TO: CD8+ lymphocyte infiltration is an independent favorable prognostic indicator in basal-like breast cancer. Breast Cancer Res 2012, 14:R48.

[30] Li H, Whitney J, Bera K, Gilmore H, Thorat MA, Badve S, Madabhushi A: Quantitative nuclear histomorphometric features are predictive of Oncotype DX risk categories in ductal carcinoma in situ: preliminary findings. Breast cancer research : BCR 2019, 21:114-.

[31] Sobral-Leite M, Salomon I, Opdam M, Kruger DT, Beelen KJ, van der Noort V, van Vlierberghe RLP, Blok EJ, Giardiello D, Sanders J, Van de Vijver K, Horlings HM, Kuppen PJK, Linn SC, Schmidt MK, Kok M: Cancer-immune interactions in ER-positive breast cancers: PI3K pathway alterations and tumor-infiltrating lymphocytes. Breast Cancer Res 2019, 21:90.

[32] Taylor CR, Levenson RM: Quantification of immunohistochemistry--issues concerning methods, utility and semiquantitative assessment II. Histopathology 2006, 49:411-24.

[33] Sukswai N, Khoury JD: Immunohistochemistry Innovations for Diagnosis and Tissue-Based Biomarker Detection. Curr Hematol Malig Rep 2019, 14:368-75.

[34] Li XF, Gruosso T, Zuo DM, Omeroglu A, Meterissian S, Guiot MC, Salazar A, Park M, Levine H: Infiltration of CD8(+) T cells into tumor cell clusters in triple-negative breast cancer. P Natl Acad Sci USA 2019, 116:3678-87.
[35] Baker K, Lachapelle J, Zlobec I, Bismar TA, Terracciano L, Foulkes WD: Prognostic significance of CD8+ T lymphocytes in breast cancer depends upon both oestrogen receptor status and histological grade. Histopathology 2011, 58:1107-16.
[36] Oda N, Shimazu K, Naoi Y, Morimoto K, Shimomura A, Shimoda M, Kagara N, Maruyama N, Kim SJ, Noguchi S: Intratumoral regulatory T cells as an independent predictive factor for pathological complete response to neoadjuvant paclitaxel followed by 5-FU/epirubicin/cyclophosphamide in breast cancer patients. Breast Cancer Res Treat 2012, 136:107-16.
[37] Dieci MV, Mathieu MC, Guarneri V, Conte P, Delaloge S, Andre F, Goubar A: Prognostic and predictive value of tumor-infiltrating lymphocytes in two phase III randomized adjuvant breast cancer trials. Ann Oncol 2015, 26:1698-704.
[38] Krishnamurti U, Wetherilt CS, Yang J, Peng L, Li X: Tumor-infiltrating lymphocytes are significantly associated with better overall survival and disease-free survival in triple-negative but not estrogen receptor-positive breast cancers. Human pathology 2017, 64:7-12.
[39] Loi S, Sirtaine N, Piette F, Salgado R, Viale G, Van Eenoo F, Rouas G, Francis P, Crown JP, Hitre E, de Azambuja E, Quinaux E, Di Leo A, Michiels S, Piccart MJ, Sotiriou C: Prognostic and predictive value of tumor-infiltrating lymphocytes in a phase III randomized adjuvant breast cancer trial in node-positive breast cancer comparing the addition of docetaxel to doxorubicin with doxorubicin-based chemotherapy: BIG 02-98. J Clin Oncol 2013, 31:860-7.
[40] Krijgsman D, Leeuwen MV, van der Ven J, Almeida V, Vlutters R, Halter D, Kuppen P, Velde CV, Wimberger-Friedl R: Quantitative whole slide assessment of tumor-infiltrating CD8-positive lymphocytes in ER-positive breast cancer in relation to clinical outcome. IEEE J Biomed Health Inform 2020, Pp.
[41] Madabhushi A: Digital pathology image analysis: opportunities and challenges. Imaging Med 2009, 1:7-10.

[42] Belsare A, Mushrif M: Histopathological image analysis using image processing techniques: An overview. Signal & Image Processing 2012, 3:23.
[43] Laurinavicius A, Laurinaviciene A, Dasevicius D, Elie N, Plancoulaine B, Bor C, Herlin P: Digital image analysis in pathology: benefits and obligation. Analytical cellular pathology 2012, 35:75-8.
[44] Laurinavicius A, Plancoulaine B, Rasmusson A, Besusparis J, Augulis R, Meskauskas R, Herlin P, Laurinaviciene A, Abdelhadi Muftah AA, Miligy I, Aleskandarany M, Rakha EA, Green AR, Ellis IO: Bimodality of intratumor Ki67 expression is an independent prognostic factor of overall survival in patients with invasive breast carcinoma. Virchows Arch 2016, 468:493-502.
[45] Plancoulaine B, Laurinaviciene A, Herlin P, Besusparis J, Meskauskas R, Baltrusaityte I, Iqbal Y, Laurinavicius A: A methodology for comprehensive breast cancer Ki67 labeling index with intra-tumor heterogeneity appraisal based on hexagonal tiling of digital image analysis data. Virchows Archiv 2015, 467:711-22.
[46] Besusparis J, Plancoulaine B, Rasmusson A, Augulis R, Green AR, Ellis IO, Laurinaviciene A, Herlin P, Laurinavicius A: Impact of tissue sampling on accuracy of Ki67 immunohistochemistry evaluation in breast cancer. Diagn Pathol 2016, 11:82.
[47] Linette GP, Carreno BM: Tumor-Infiltrating Lymphocytes in the Checkpoint Inhibitor Era. Current hematologic malignancy reports 2019, 14:286-91.
[48] Nagarajan D, McArdle SEB: Immune Landscape of Breast Cancers. Biomedicines 2018, 6.
[49] Campbell MJ, Scott J, Maecker HT, Park JW, Esserman LJ: Immune dysfunction and micrometastases in women with breast cancer. Breast Cancer Res Treat 2005, 91:163-71.
[50] Salmaninejad A, Valilou SF, Shabgah AG, Aslani S, Alimardani M, Pasdar A, Sahebkar A: PD-1/PD-L1 pathway: Basic biology and role in cancer immunotherapy. J Cell Physiol 2019, 234:16824-37.
[51] Adams S, Card D, Zhao J, Karantza V, Aktan G: Abstract OT1-03-20: A phase 2 study of pembrolizumab (MK-3475) monotherapy for metastatic triple-negative breast cancer

(mTNBC): KEYNOTE-086. Cancer Research 2016, 76:OT1-03-20-OT1-03-20.
[52] Dirix LY, Takacs I, Jerusalem G, Nikolinakos P, Arkenau HT, Forero-Torres A, Boccia R, Lippman ME, Somer R, Smakal M, Emens LA, Hrinczenko B, Edenfield W, Gurtler J, von Heydebreck A, Grote HJ, Chin K, Hamilton EP: Avelumab, an anti-PD-L1 antibody, in patients with locally advanced or metastatic breast cancer: a phase 1b JAVELIN Solid Tumor study. Breast Cancer Res Treat 2018, 167:671-86.
[53] Emens LA, Braiteh FS, Cassier P, Delord J-P, Eder JP, Fasso M, Xiao Y, Wang Y, Molinero L, Chen DS, Krop I: Abstract 2859: Inhibition of PD-L1 by MPDL3280A leads to clinical activity in patients with metastatic triple-negative breast cancer (TNBC). Cancer Research 2015, 75:2859-.
[54] Nanda R, Chow LQ, Dees EC, Berger R, Gupta S, Geva R, Pusztai L, Pathiraja K, Aktan G, Cheng JD, Karantza V, Buisseret L: Pembrolizumab in Patients With Advanced Triple-Negative Breast Cancer: Phase Ib KEYNOTE-012 Study. J Clin Oncol 2016, 34:2460-7.
[55] Rugo H, Delord J-P, Im S-A, Ott P, Piha-Paul S, Bedard P, Sachdev J, Le Tourneau C, van Brummelen E, Varga A, Saraf S, Pietrangelo D, Karantza V, Tan A: Abstract S5-07: Preliminary efficacy and safety of pembrolizumab (MK-3475) in patients with PD-L1–positive, estrogen receptor-positive (ER+)/HER2-negative advanced breast cancer enrolled in KEYNOTE-028. Cancer Research 2016, 76:S5-07-S5-.
[56] Rasmusson A, Zilenaite D, Nestarenkaite A, Augulis R, Laurinaviciene A, Ostapenko V, Poskus T, Laurinavicius A: Immunogradient indicators for anti-tumor response assessment by automated tumor-stroma interface zone detection. The American Journal of Pathology 2020.
[57] Zilenaite D, Rasmusson A, Augulis R, Besusparis J, Laurinaviciene A, Plancoulaine B, Ostapenko V, Laurinavicius A: Independent Prognostic Value of Intratumoral Heterogeneity and Immune Response Features by Automated Digital Immunohistochemistry Analysis in Early Hormone Receptor-Positive Breast Carcinoma. Frontiers in Oncology 2020, 10.
[58] Haralick RM: Statistical and structural approaches to texture. Proceedings of the IEEE 1979, 67:786-804.

[59] Xuan G, Zhang W, Chai P: EM algorithms of Gaussian mixture model and hidden Markov model. Proceedings 2001 International Conference on Image Processing (Cat No 01CH37205): IEEE, 2001. pp. 145-8.
[60] Dempster AP, Laird NM, Rubin DB: Maximum likelihood from incomplete data via the EM algorithm. Journal of the Royal Statistical Society: Series B (Methodological) 1977, 39:1-22.
[61] Samuels P: Advice on Exploratory Factor Analysis, 2017.
[62] Kaiser HF: An index of factorial simplicity. Psychometrika 1974, 39:31-6.
[63] Hair J, Black W, Babin B, Anderson R, Tatham R: Multivariate Data Analysis. 6 ed. Upper Saddle River: Pearson Prentice Hall, 2006.
[64] Budczies J, Klauschen F, Sinn BV, Gyorffy B, Schmitt WD, Darb-Esfahani S, Denkert C: Cutoff Finder: a comprehensive and straightforward Web application enabling rapid biomarker cutoff optimization. PLoS One 2012, 7:e51862.
[65] Parzen M, Lipsitz SR: A global goodness-of-fit statistic for Cox regression models. Biometrics 1999, 55:580-4.
[66] Rushing C, Bulusu A, Hurwitz HI, Nixon AB, Pang H: A leave-one-out cross-validation SAS macro for the identification of markers associated with survival. Computers in Biology and Medicine 2015, 57:123-9.
[67] Bordry N, Broggi MAS, de Jonge K, Schaeuble K, Gannon PO, Foukas PG, Danenberg E, Romano E, Baumgaertner P, Fankhauser M, Wald N, Cagnon L, Abed-Maillard S, Hajjami HM, Murray T, Ioannidou K, Letovanec I, Yan P, Michielin O, Matter M, Swartz MA, Speiser DE: Lymphatic vessel density is associated with CD8(+) T cell infiltration and immunosuppressive factors in human melanoma. Oncoimmunology 2018, 7:e1462878.
[68] Hermitte F: Biomarkers immune monitoring technology primer: Immunoscore® Colon. J Immunother Cancer 2016, 4:57.
[69] Lechner A, Schlosser H, Rothschild SI, Thelen M, Reuter S, Zentis P, Shimabukuro-Vornhagen A, Theurich S, Wennhold K, Garcia-Marquez M, Tharun L, Quaas A, Schauss A, Isensee J, Hucho T, Huebbers C, von Bergwelt-Baildon M, Beutner D: Characterization of tumor-associated T-lymphocyte subsets and

immune checkpoint molecules in head and neck squamous cell carcinoma. Oncotarget 2017, 8:44418-33.
[70] Stanton SE, Adams S, Disis ML: Variation in the Incidence and Magnitude of Tumor-Infiltrating Lymphocytes in Breast Cancer Subtypes: A Systematic Review. JAMA Oncol 2016, 2:1354-60.
[71] Savas P, Salgado R, Denkert C, Sotiriou C, Darcy PK, Smyth MJ, Loi S: Clinical relevance of host immunity in breast cancer: from TILs to the clinic. Nat Rev Clin Oncol 2016, 13:228-41.
[72] Kurozumi S, Matsumoto H, Kurosumi M, Inoue K, Fujii T, Horiguchi J, Shirabe K, Oyama T, Kuwano H: Prognostic significance of tumour-infiltrating lymphocytes for oestrogen receptor-negative breast cancer without lymph node metastasis. Oncol Lett 2019, 17:2647-56.
[73] Salgado R, Denkert C, Campbell C, Savas P, Nuciforo P, Aura C, de Azambuja E, Eidtmann H, Ellis CE, Baselga J, Piccart-Gebhart MJ, Michiels S, Bradbury I, Sotiriou C, Loi S: Tumor-Infiltrating Lymphocytes and Associations With Pathological Complete Response and Event-Free Survival in HER2-Positive Early-Stage Breast Cancer Treated With Lapatinib and Trastuzumab: A Secondary Analysis of the NeoALTTO Trial. JAMA Oncology 2015, 1:448-55.
[74] Ali HR, Provenzano E, Dawson SJ, Blows FM, Liu B, Shah M, Earl HM, Poole CJ, Hiller L, Dunn JA, Bowden SJ, Twelves C, Bartlett JM, Mahmoud SM, Rakha E, Ellis IO, Liu S, Gao D, Nielsen TO, Pharoah PD, Caldas C: Association between CD8+ T-cell infiltration and breast cancer survival in 12,439 patients. Ann Oncol 2014, 25:1536-43.
[75] Lee KH, Kim EY, Yun JS, Park YL, Do SI, Chae SW, Park CH: The prognostic and predictive value of tumor-infiltrating lymphocytes and hematologic parameters in patients with breast cancer. BMC Cancer 2018, 18:938.
[76] Han HJ, Russo J, Kohwi Y, Kohwi-Shigematsu T: SATB1 reprogrammes gene expression to promote breast tumour growth and metastasis. Nature 2008, 452:187-93.
[77] Galande S, Purbey PK, Notani D, Kumar PP: The third dimension of gene regulation: organization of dynamic chromatin loopscape by SATB1. Curr Opin Genet Dev 2007, 17:408-14.

[78] Kohwi-Shigematsu T, Kohwi Y, Takahashi K, Richards HW, Ayers SD, Han HJ, Cai S: SATB1-mediated functional packaging of chromatin into loops. Methods 2012, 58:243-54.
[79] Kohwi-Shigematsu T, Poterlowicz K, Ordinario E, Han HJ, Botchkarev VA, Kohwi Y: Genome organizing function of SATB1 in tumor progression. Semin Cancer Biol 2013, 23:72-9.
[80] Glatzel-Plucinska N, Piotrowska A, Dziegiel P, Podhorska-Okolow M: The Role of SATB1 in Tumour Progression and Metastasis. Int J Mol Sci 2019, 20.
[81] Cai S, Han HJ, Kohwi-Shigematsu T: Tissue-specific nuclear architecture and gene expression regulated by SATB1. Nat Genet 2003, 34:42-51.
[82] Iorns E, Hnatyszyn HJ, Seo P, Clarke J, Ward T, Lippman M: The role of SATB1 in breast cancer pathogenesis. J Natl Cancer Inst 2010, 102:1284-96.
[83] Selinger CI, Cooper WA, Al-Sohaily S, Mladenova DN, Pangon L, Kennedy CW, McCaughan BC, Stirzaker C, Kohonen-Corish MR: Loss of special AT-rich binding protein 1 expression is a marker of poor survival in lung cancer. J Thorac Oncol 2011, 6:1179-89.
[84] Patani N, Jiang W, Mansel R, Newbold R, Mokbel K: The mRNA expression of SATB1 and SATB2 in human breast cancer. Cancer Cell Int 2009, 9:18.
[85] Hanker LC, Karn T, Mavrova-Risteska L, Ruckhäberle E, Gaetje R, Holtrich U, Kaufmann M, Rody A, Wiegratz I: SATB1 gene expression and breast cancer prognosis. Breast 2011, 20:309-13.
[86] Ahlfors H, Limaye A, Elo LL, Tuomela S, Burute M, Gottimukkala KV, Notani D, Rasool O, Galande S, Lahesmaa R: SATB1 dictates expression of multiple genes including IL-5 involved in human T helper cell differentiation. Blood 2010, 116:1443-53.
[87] Satoh Y, Yokota T, Sudo T, Kondo M, Lai A, Kincade PW, Kouro T, Iida R, Kokame K, Miyata T, Habuchi Y, Matsui K, Tanaka H, Matsumura I, Oritani K, Kohwi-Shigematsu T, Kanakura Y: The Satb1 protein directs hematopoietic stem cell differentiation toward lymphoid lineages. Immunity 2013, 38:1105-15.

[88] Alvarez JD, Yasui DH, Niida H, Joh T, Loh DY, Kohwi-Shigematsu T: The MAR-binding protein SATB1 orchestrates temporal and spatial expression of multiple genes during T-cell development. Genes Dev 2000, 14:521-35.
[89] Kakugawa K, Kojo S, Tanaka H, Seo W, Endo TA, Kitagawa Y, Muroi S, Tenno M, Yasmin N, Kohwi Y, Sakaguchi S, Kowhi-Shigematsu T, Taniuchi I: Essential Roles of SATB1 in Specifying T Lymphocyte Subsets. Cell Rep 2017, 19:1176-88.
[90] Stephen TL, Payne KK, Chaurio RA, Allegrezza MJ, Zhu H, Perez-Sanz J, Perales-Puchalt A, Nguyen JM, Vara-Ailor AE, Eruslanov EB, Borowsky ME, Zhang R, Laufer TM, Conejo-Garcia JR: SATB1 Expression Governs Epigenetic Repression of PD-1 in Tumor-Reactive T Cells. Immunity 2017, 46:51-64.
[91] Laurinavicius A, Green AR, Laurinaviciene A, Smailyte G, Ostapenko V, Meskauskas R, Ellis IO: Ki67/SATB1 ratio is an independent prognostic factor of overall survival in patients with early hormone receptor-positive invasive ductal breast carcinoma. Oncotarget 2015, 6:41134-45.
[92] Noordhoek I, de Groot AF, Cohen D, Liefers GJ, Portielje JEA, Kroep JR: Higher ER load is not associated with better outcome in stage 1-3 breast cancer: a descriptive overview of quantitative HR analysis in operable breast cancer. Breast Cancer Res Treat 2019, 176:27-36.
[93] Bartlett JM, Brookes CL, Robson T, van de Velde CJ, Billingham LJ, Campbell FM, Grant M, Hasenburg A, Hille ET, Kay C, Kieback DG, Putter H, Markopoulos C, Kranenbarg EM, Mallon EA, Dirix L, Seynaeve C, Rea D: Estrogen receptor and progesterone receptor as predictive biomarkers of response to endocrine therapy: a prospectively powered pathology study in the Tamoxifen and Exemestane Adjuvant Multinational trial. J Clin Oncol 2011, 29:1531-8.
[94] Lamy PJ, Pujol P, Thezenas S, Kramar A, Rouanet P, Guilleux F, Grenier J: Progesterone receptor quantification as a strong prognostic determinant in postmenopausal breast cancer women under tamoxifen therapy. Breast Cancer Res Treat 2002, 76:65-71.
[95] Abubakar M, Figueroa J, Ali HR, Blows F, Lissowska J, Caldas C, Easton DF, Sherman ME, Garcia-Closas M, Dowsett M, Pharoah PD: Combined quantitative measures of ER, PR, HER2,

and KI67 provide more prognostic information than categorical combinations in luminal breast cancer. Mod Pathol 2019, 32:1244-56.
[96] Purdie CA, Quinlan P, Jordan LB, Ashfield A, Ogston S, Dewar JA, Thompson AM: Progesterone receptor expression is an independent prognostic variable in early breast cancer: a population-based study. Br J Cancer 2014, 110:565-72.
[97] Andor N, Graham TA, Jansen M, Xia LC, Aktipis CA, Petritsch C, Ji HP, Maley CC: Pan-cancer analysis of the extent and consequences of intratumor heterogeneity. Nat Med 2016, 22:105-13.
[98] Qi D, Wu E: Cancer prognosis: Considering tumor and its microenvironment as a whole. EBioMedicine 2019, 43:28-9.

SUPPLEMENTARY MATERIAL

Supplementary Table 1. Summary statistics of CD8+ cell density indicators:

CD8+ cell density indicator, cell/mm^2	Mean	Standard deviation	Minimum	Maximum	Median
CD8_CM_mean	-1.06	0.79	-2.54	1.26	-1.17
CD8_CM_sd	-1.17	0.54	-2.28	0.17	-1.25
CD8_ID_mean	4.57	5.35	0.39	42.22	3.27
CD8_mean_S	210.44	198.46	8.16	1243.14	155.25
CD8_sd_S	368.52	233.33	42.26	1237.32	317.36
CD8_mean_TE	148.81	164.94	4.65	1135.39	110.01
CD8_sd_TE	259.68	158.85	28.40	846.14	213.80
CD8_mean_T	71.41	84.97	0.52	451.36	39.85
CD8_sd_T	116.85	87.96	7.23	509.79	96.92

CD8_CM_mean, the center of mass for CD8 density by mean in ranks [-4; 4]; CD8_CM_sd, the center of mass for CD8 by variance in ranks [-4; 4]; CD8_ID_mean, immunodrop of the mean of CD8+ density; CD8_mean and CD8_sd (standard deviation) are summarized in the stroma (S), TE, and tumor (T) aspect of IZ, respectively.

Supplementary Table 2. Summary statistics of immunohistochemistry and intratumoral heterogeneity indicators:

Indicator	Mean	Standard deviation	Minimum	Maximum	Median
Conventional breast cancer indicators					
ER%	68.85	25.93	0.03	98.82	78.68
PR%	38.50	34.11	0.03	96.28	31.87
HER2%	10.53	22.20	0.002	90.62	0.64
Ki67%	7.21	6.46	0.39	40.53	5.36
Intratumoral heterogeneity indicators					
ER_energy	0.24	0.28	0.02	1.00	0.14
ER_homogeneity	0.71	0.13	0.46	1.00	0.69
ER_entropy	3.48	1.53	0	6.00	3.67
ER_contrast	1.95	1.21	0	5.18	1.90
ER_dissimilarity	0.77	0.38	0	1.61	0.76
ER_AshD	3.36	9.24	0.82	93.12	1.86
PR_energy	0.42	0.40	0.02	1.00	0.15
PR_homogeneity	0.76	0.18	0.42	1.00	0.72
PR_entropy	2.93	2.14	0	6.02	3.63
PR_contrast	1.76	1.69	0	7.25	1.68
PR_dissimilarity	0.65	0.53	0	1.87	0.78
PR_AshD	2.30	2.03	0.15	14.41	1.86
Ki67_energy	0.66	0.31	0.05	1.00	0.72
Ki67_homogeneity	0.91	0.10	0.58	1.00	0.94
Ki67_entropy	1.13	1.10	0	4.80	0.87
Ki67_contrast	0.24	0.36	0	2.29	0.13
Ki67_dissimilarity	0.19	0.21	0	1.01	0.12
Ki67_AshD	2.08	1.30	0	7.05	1.71
Immune response indicators					
CD8_d_S	209.25	199.07	8.16	1243.14	152.95
CD8_d_T	70.72	85.03	0.52	451.36	37.39
CD8_SATB1_d_S	54.11	78.70	0.56	541.47	28.41
CD8_SATB1_d_T	14.99	25.87	0	160.82	5.47
Hypoxia-inducible indicators					
HIF1α%_S	0.46	0.65	0.04	4.29	0.28
HIF1α%_T	0.16	0.37	0.01	3.16	0.06

AshD, Ashman's D; d, density; S, stroma part; T, tumor part.

Supplementary Table 3. Results of leave-one-out cross-validation analyzing different sets of Haralick's texture indicators of estrogen receptor (ER), progesterone receptor (PR), and Ki67 together with clinical and pathological, conventional breast cancer immunohistochemistry biomarkers, immune response, hypoxia-inducible indicators:

Haralick's texture indicator	Selected variables in Cox regression model	Frequency of the Cox regression model repeats	$\chi 2$ of Cox regression model	*p*-value
Energy	CD8_d_T HIF1α%_S Ki67_AshD PR_energy	55	8.03	0.0016
Homogeneity	pN group (pN0 and pN1-3) CD8_d_S Ki67_AshD PR_homogeneity	56	8.12	0.0002
Entropy	CD8_SATB1_d_T Ki67_AshD PR_entropy	61	10.03	0.0015
Contrast	CD8_SATB1_d_T Ki67_AshD PR_contrast	51	9.74	0.0019
Dissimilarity	CD8_d_T HIF1α_S Ki67_dissimilarity PR_dissimilarity	53	5.72	0.017

AshD, Ashman's D; d, density; S, stroma part; T, tumor part; pN, lymph node metastasis status.

Vilnius University Press
9 Saulėtekio Ave., Building III, LT-10222 Vilnius
Email: info@leidykla.vu.lt, www.leidykla.vu.lt
Print run 25